Aerodynamic performance increase over an A320 morphing wing in transonic regime by numerical simulation at high Reynolds number

Jacques Abou Khalil, César Jiménez Navarro, Rami El Jeaid, Abderahmane Marouf, Rajaa El Akoury, Yannick Hoarau, Jean-François Rouchon, Marianna Braza

Aerodynamic performance increase over an A320 morphing wing in transonic regime by numerical simulation at high Reynolds number

J. Abou-Khalil[3,1], C. Jimenez-Navarro[1], R. El Jeaid[1], A. Marouf[1,2], R. El Akoury[1], Y. Hoarau[2], J.F. Rouchon[3] and M. Braza[1]

[1]*IMFT Institut de Mécanique des Fluides de Toulouse, Unité Mixte C.N.R.S.-I.N.P.T. 5502, All. du Prof. Camille Soula, 31400 Toulouse, France*

[2]*ICUBE Laboratoire des sciences de l'Ingénieur, de l'Informatique et de l'Imagerie, UMR 7357 CNRS-Univ. Strasbourg ENGEES-INSA 4 Rue Blaise Pascal, 67081, Strasbourg, France*

[3]*LAPLACE Laboratoire Plasma et Conversion d'Energie, UMR 5213 CNRS-INPT-UT3 2 Rue Charles Camichel, 31071 Toulouse, France*

Abstract

This article investigates the aerodynamic performance increase of an Airbus A320 morphing aerofoil, having a chord of 70cm at Mach number 0.78 corresponding to cruise conditions and Reynolds number of 4.5×10^6. The morphing concepts involved vibration and slight deformation of the trailing edge region as well as actuation through travelling waves (TW) along a specific area of the suction side. These morphing concepts are integrated on the wing prototypes studied under the French "Agence Nationale de Recherche"-ANR project EMBIA - "Electrical Multiscale Bioinspired Interfaces in Aeronautics", https://anr.fr/Project-ANR-21-CE05-0006 and in the context of the H2020 European project TEAMAERO, ("Towards Effective Flow Control and Mitigation of Shock Effects in Aeronautical Applications") (https://cordis.europa.eu/project/id/860909/fr). The present paper analyses by means of numerical simulation the physical mechanisms leading to the increase of the lift-to-drag ratio as well as the drag and noise sources reduction. Frequency vibrations ranging from 250 Hz to 750 Hz and amplitudes in the order of 1 mm have been examined. Three angles of attack have been considered regarding the Trailing Edge (TE) actuation: 0°, 1.8°, and 2.4°, as well as the angle of 1.8° for the Travelling Wave (TW) actuation. This study analysed how these morphing concepts take advantage of feedback effects stemming from the near wake unsteadiness towards the Shock Boundary Layer Interaction (SBLI) region and even upstream of it and the reasons for obtaining a considerable aerodynamic performance increase. Among them, a lock-in mechanism of the transonic buffet oscillations on the vibration frequency has been obtained leading to a considerable lift-to-drag ratio and mitigation of the transonic buffet instability. These facts led to a drag reduction of 14% and an increase in aerodynamic efficiency (lift-to-drag ratio) by approximately 12 %.

Key words: Transonic flow, morphing, A320 wing, buffet, SBLI, aerodynamics.

1 Introduction

Understanding the principal mechanisms related to buffet instabilities and their interaction with the shear layers and the near wake unsteadiness in the transonic regime around a supercritical airfoil, to successfully modify them through electroactive morphing is the main objective of this paper. Under certain conditions, aircraft wings in the transonic Mach number range of (0.7 - 0.8) may experience an amplification of a low frequency-high amplitude instability of the shock wave that moves periodically along a specific area on the lifting structure. This leads to a drastic drag increase and may create triggering conditions for amplification of harmful dip-flutter modes. Pioneering studies of Seegmiller *et al.* (1978), McDevitt *et al.* (1976), Levy (1978), Marvin *et al.* (1980) and Jacquin *et al.* (2005, 2009) made evidence and analysed the transonic buffet phenomenon. This periodic "excursion" of the shock wave occurs along the suction and pressure sides in case of symmetric airfoil sections and along the suction side only in case of supercritical wing sections as the one of the A320 that concerns the present study.

A considerable number of numerical studies were devoted in the prediction and physical analysis of the transonic buffet. Deck (2005), using the Zonal Detached Eddy Simulations (ZDES), and Brunet (2003), Brunet *et al* (2005), employing URANS, were performed on similar configurations. Furthermore, a DDES approach using the SALSA – "Strain adaptive linear Spalart-Allmaras model" by Rung *et al.* (2003) for the near wall region was applied by Grossi *et al.* (2014) on the OAT15A wing in the context of the European research program ATAAC, "Advanced Turbulent simulations for Aerodynamic Application Challenges", https://cordis.europa.eu/project/id/233710. This study, as well as the study by S. Deck (2005) has shown the reduction of the well known "grey area" effects between the URANS and LES regions that occur in the DDES and create a "Massive Stress Depletion", (MST), thanks to these modelling approaches. The LES simulations by Dandois (2018) have shown through phase-averaged fields a linking of the transonic buffet frequency to a separation bubble "breathing" phenomenon associated with a vortex shedding mechanism. Furthermore, Paladini *et al.* (2019) simulated three-dimensional buffet cells along a swept wing configuration.

An illustration of the transonic buffet among first experimental visualisations by Schlieren approach is shown in figure 1 (left) and through numerical simulation as for example in figure 1 (right). In both parts of this figure, the Shock-Boundary Layer Interaction (SBLI) is shown forming a "lambda" structure in the shock foot, as well as the development of the separated shear layers containing small-scale shear-layer vortices, the Kelvin-Helmholtz (KH) ones that lead farther downstream to the alternating von Kármán vortices. In-between these vortex structures, smaller scale chaotic eddies are formed due to the turbulence. There is also shown that secondary waves are formed on the "crests" of these vortices along the shear layers as well as upstream of the shock, because of the thickening of the so-called "effective obstacle", which is not the nominal profile's shape but the one countered by the shearing regions. For the same reasons, an oblique shock just upstream of the lambda foot is created, because of the flow reversal that goes even under the shock's foot towards this upstream area and creates there a local thickening of the boundary layer, thus producing this secondary shock. This pattern was shown in a number of experimental studies in the collected contributions of the European research project TFAST, "Transition Location effect on shock boundary layer interaction" https://cordis.europa.eu/project/id/265455, (Doerffer *et al.* 2021). Therefore, a significant feedback effect from this downstream unsteadiness towards the area

upstream of the shock can be seen.

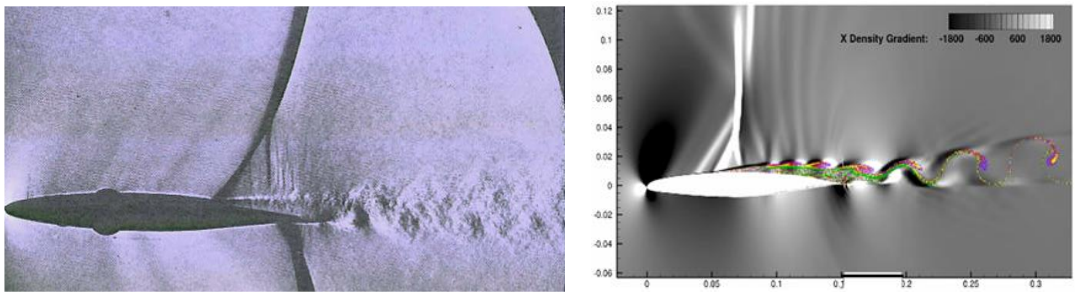

Figure 1: Normal shock wave and instabilities in transonic flow. Left: Schlieren photograph of the eddying wake following a shock-induced flow separation (Courtesy of National Physical Laboratory, England; study by Duncan *et al.* (1932); photo by D.W. Holder, in Fung (2002)). Right: streak-line visualization from simulations by Tô *et al.* (2019) illustrating the SBLI, the shear layer and von Kármán vortices. Both correspond to transonic buffet cases.

The importance of the near wake unsteadiness in affecting the transonic buffet studied by numerical simulations (Jimenez-Garcia (2012), Szubert *et al.* (2012)), regarding the OAT15A supercritical aerofoil at Reynolds number of 3 million by introducing a splitter-plate at the trailing edge, which suppressed the von Kármán mode. It was shown that in the cases where the von Kármán mode was remote (downstream of a critical length of the splitter plate), the buffet mode was considerably attenuated and disappeared. The influence of the shear layers and near wake unsteadiness was further analysed by Szubert *et al.* (2015), by means of an appropriate turbulence modelling closure sensitized for the coherent structures development where a slight injection of low energy small vortices in the shear layers through Proper Orthogonal Decomposition (POD) and stochastic forcing, produced a considerable thinning of these shear layers and modified the upstream dynamics of the transonic buffet, yielding improved evaluation of the pressure distribution and of the forces around the OAT15A aerofoil in the same Reynolds number range. The strong influence and inter-dependence of the downstream unsteadiness on the shock's motion was studied in more details through unsteady Navier-Stokes simulations by (Bouhadji and Braza (2003a, 2003b) in the lower Reynolds number range in the order of 10,000, where the time and length scales permitted a more focused identification of the shock-vortex interaction, as well as in the DNS studies by Bourdet *et al.* (2003).

This inter-dependence is highly used in the present study for the attenuation or even suppression of the buffet through adequate and novel morphing concepts by manipulating the separated shear layers and near trailing edge region unsteadiness as discussed in the following sections.

When the Mach number increases in the range of (0.85 - 0.9), or when the regime becomes supersonic, the shock wave is pushed farther downstream, near or beyond the trailing edge and acts as a barrier to the near wake perturbations travelling upstream, because of the enhancement of the hyperbolic character of the flow, as shown by Bouhadji and Braza (2003a) . Therefore, in the higher transonic Mach number range or beyond, no more buffet instability occurs. These different regimes depend on the wing's form and on the chord's length related to the Mach and Reynolds number. In addition, in the case of swept wings where the chord varies as a function of the span, part of the span sections are under-critical concerning buffet and part of them over-critical, as studied by Tô *et al.* (2019), as shown in the context of the TFAST EU project, for the swept V2C wing of Dassault Aviation (Szubert *et al.* (2021)) at Reynolds numbers in the order of 12 million.

The development of the shear layer and near wake instabilities increase the width of the wake, forcing the shock to move upstream and enhance the onset of buffet, responsible for a considerable drag reduction and loss of lift, harmful for the aerodynamic performance. These facts highlight the need to study in detail the mechanisms associated to the shock wave movement that involves a fast change in pressure, to control these harmful effects through modification of the near trailing edge unsteadiness. This goal is accomplished in the present article through electroactive morphing thanks to novel actuators, whose a first part has been studied in the H2020 N° 723402 European project SMS, "Smart Morphing and Sensing for aeronautical configurations", https://cordis.europa.eu/project/id/723402/fr and www.smartwing.org/SMS/EU (collected studies can be found in the book by Braza *et al.* (2023).

Although the current wing shapes are non-deformable, there is an increased interest during the last decade in bioinspired aircraft design where disruptive aircraft configurations are considered to remove these harmful effects and simultaneously to reduce the noise sources produced past the trailing edge thus providing lighter, safer, environmentally friendly aircraft transport and cost-effective solutions. To increase the aerodynamic performance of airplanes, researchers have investigated the concept of wing morphing. The idea of adaptable wings has roots in historical aviation developments, such as Clément Ader's "Eole," which made a brief flight in 1890 and is currently on display at the Centre National des Arts et Métiers (CNAM) Museum in Paris. Ader's designs were influenced by birds and bats deformable wings. Similarly, the Wright brothers' first airplane demonstrating a sustainable flight in 1903 incorporated flexible wings, marking the beginning of a transformative era in aviation history.

The interest on deformable lifting structures has been brought back by recent developments in materials science and actuation technologies (Namgoong *et al.* (2007)). The performance ranges of conventional wing shape control and adaptation techniques, such as slats and flaps, are constrained Barbarino *et al.* (2011).

An example of deformable wing structure was presented at the Royal International Air Tatto air show in the United Kingdom as the bird-like aircraft known as bird of prey (https://www.airbus.com/en/newsroom), a new conceptual airliner for regional transportation. This partly bio-inspired design comes from efficient mechanics of eagles by applying technologies of hybrid-electric propulsion, active control systems, and advances composite structures. Wings (slats, flaps and winglets) and tails mimic those of a bird of prey with added feathers for an active flight control. Another example is the Albatross One airplane constructed by AIRBUS with articulated wing tips inspired from the Albatross bird. This is a first aircraft demonstrator to perform freely flapping wing-tips that can react and flex to wind strong changes like gusts and significantly alleviate loads and drag for a lighter, more fuel-efficient aircraft. It was demonstrated that cambering of the wing can be efficient, Lyu and Martins (2015) in the framework of aircraft or for the Unmanned Aerial Vehicle (UAV) applications, Zhao et al. (2019) aerodynamic efficiency improvements. Different cambering approaches were proposed through the spanwise direction, Tawfik et al. (2011) imitating biologically inspired morphing wings.

A number of researchers proposed smooth deformable structures stated in Woods and Friswell (2015) such as Parker (1920), Antoni (1932), Bryant and Stewart (1963), Zapel (1978), Campanile and Sachau (2000), Bartley-Cho *et al.* (2004). More recently, among international projects, the research programs Smart Intelligent Aircraft Structures "SARISTU", Wölcken and Papadopoulos (2016), Dimino *et al.* (2016) and Pecora *et al.* (2016) used adaptative leading-edge and new innovative winglet system with trailing-edge adaptation described as wing-compliant morphing. Furthermore, by using Shape Memory

Alloy (SMA), a 16 % semi-span model wing twist was accomplished in the context of studies by NASA DARPA ("Defense Advanced Research Projects Agency)" Smart Wing program, where rolling moment and lift were both improved by 8 % in comparison to the non-deformable wing (McGowan *et al*. (1998)). In addition, NASA has worked with the US Air Force research laboratory and FlexSys on the Adaptative Compliant Trailing Edge "ACTE" project, to construct an advanced design of a flap able to make deflection in the downward and upward directions during take-off and landing phases to increase the aerodynamic performances. The experiment was conducted on a modified Glufstream III (G-III) a business jet that was changed into an aerodynamic research test bench at Armstrong Flight Research Center of NASA Cruz and Miller (2016). Flight tests were conducted in this project, described in Kota et al. (2016). This solution revealed to yield aerodynamic benefits. These new adaptative structures were actuated through conventional actuators similarly as servomotors that introduce a significant additional mass to the wing. In the European project AFLoNext, hybrid laminar wing design through a Krüger concept of the leading edge compensated the loss of 5 % lift due to the wing/pylon interaction. In this project, AFC (Active Flow Control) on wing trailing edges provided a 1-2 % fuel saving while HLFC (Hybrid Laminar Flow Control technology) gave 9 % fuel savings. However, the devices used up to now use in the majority electromechanical and/or hydraulic-driven actuators and MEMS systems that are heavy and slow in response.

The multidisciplinary research team of IMFT ("Institut de Mécanique des Fluides de Toulouse") and LAPLACE ("Laboratoire Plasma et Conversion d'Energie") introduced novel morphing concepts in the context of the STAE "Sciences et Technologies pour l'Aéronautique et l'Espace" (http://www.fondation-stae.net/) Foundation through federative research projects since 2010, EMMAV - "Electroactive Morphing for Micro-Airvehicles" and DYNAMORPH - "DYNAmic regime electroactive MORPHing" as well as the creation of the research platform SMC - "Smart Morphing Centre", www.smartwing.org. The use of Shape Memory Alloys (SMA) in the EMMAV project was explored by Chinaud *et al.* (2012), (2013) and (2014), focusing on the capacity of obtaining a substantial deformation of a plate in the Reynolds number range of (200,000-500,000). The deformation was obtained by means of transformation of the electrical energy supply to Joule effect through the heating of the SMA wires according a thermo-mechanical law. Wind-tunnel experiments were performed in this study using Time Resolved Particle Image Velocimetry (TRPIV). They explored for the first time in the literature the modification of the turbulence stresses through the SMA morphing. The shear layer modification past the trailing-edge was examined as a function of the electrical intensity for the SMA actuation.

To effectively manipulate the multiple time and length scales governing the turbulence spectrum multifaceted nature, different kinds of electrical actuators have been embeded in the lifting structure, able to actuate it at different frequencies and deformation amplitudes, simultaneously, under the so-called "hybrid electroactive morphing" concept, Scheller *et al* (2016), Scheller (2015) on a NACA4412 wing by employing Shape Memory Alloys (SMA) to induce significant deformations at low frequencies (around 1 Hz) across a major portion of the wing and simultaneously, trailing edge vibrations in the frequency range of 50-500 Hz, coupled with small deformations in the order of 1-2 mm through piezo actuators of the MFC type ("Macro-Fiber Composites"). This concept led to aerodynamic performance increase in the order of 5 %. In the Reynolds number range (200,000 - 400,000), Scheller et al (2015) studied the vibration effects on a NACA0012 aileron through a "push-push" actuator system and obtained a significant vortex breakdown and attenuation of the shear layer vortices yielding a considerable reduction of the wake's width and a practical suppression of the shear layer instability amplitude. (Jodin *et al.* (2017)) applied the hybrid

electroactive morphing concept on an A320 morphing wing prototype at Reynolds number of 1 million and shown that the TE actuation is able to add an order of 2 % of lift increase. Piezoelectric stack actuators used in other studies include flex tension actuators and enhanced piezoelectric stacks by LeLetty *et al.* (2002), among other.

Numerical studies that obtained manipulation of the transonic buffet through these kinds of electroactive morphing have been accomplished by Tô *et al.* (2019) using trailing edge actuation on an Airbus A320 morphing wing prototype with a 15 cm chord length at Reynolds number in the order of 2 million. This study produced a drag reduction in the order of 9 % and a lift increase in the order of 5 % and a drag reduction in the order of 9 % by using an association of a slight upwards deflection by 1° of the near trailing edge region and a simultaneous vibration of 90 Hz. This study depicted a "lock-in" effect of the shock wave on the actuation frequency for the first time in the literature. IMFT actively participated in European research projects related to transonic interaction, including UFAST ("Unsteady effect on shock wave-induced separation") (https://cordis.europa.eu/project/id/12226/reporting/fr), Doerffer *et al* (2011) and TFAST EU project, https://cordis.europa.eu/project/id/265455, (Doerffer *et al*. 2021). as well as in the EU-TEAMAERO project (https://cordis.europa.eu/project/id/860909/fr). These studies covered a range of Mach and Reynolds numbers and aimed at controlling the harmful instabilities arising in cruise conditions, as the transonic buffet one. Moreover, in the SMS EU project (https://cordis.europa.eu/project/id/723402/fr) coordinated by IMFT a number of studies were devoted in the mitigation of the buffet instability by implementing trailing edge vibration in the so-called tRS "transonic Reduced Scale A320 wing prototype of 15 cm chord length. Experiments were conducted in the corresponding wind tunnel dimensions of the Laboratory IMP-PAN in Gdańsk, partner in the SMS project. The morphing prototype used for these experiments was provided by the LAPLACE laboratory. Optimal trailing edge actuation approaches were determined through numerical studies conducted at IMFT (Tô *et al.* (2019)) as previously mentioned. The experiments shown an order of 4 % of drag reduction and a 3 % of lift increase for an actuation frequency of 300 Hz at Mach number of 0.78 and angle of attack (AoA) of 1.8° (values suggested by AIRBUS-France, endorser of the SMS project). The simulations along a large number of frequencies in the range of (100, 750) Hz and Reynolds number in the order of 2 million, have shown a drag reduction in the order of 9 % and a lift increase in the order of 5 % (Braza *et al.* (2023). The most interesting actuation frequencies and amplitudes obtained in these previous studies have been selected to be examined in the present article.

Based on these previous works, the present one seeks to study the morphing effects on a larger prototype with a 70 cm chord length, to approach more closer design conditions. This study examines Trailing Edge (TE) actuation at selected vibration frequencies from the previous study and a novel approach introduced for the first time in the transonic regime, the creation of "Travelling Waves", (TW) along strategic areas of the suction side. It is important to note that experiments in the transonic regime involving such dimensions are relatively rare and expensive. Therefore, numerical studies play a crucial role in identifying the optimal ranges of vibration frequencies and actuation amplitudes. In this context, the current study has been undertaken as a continuation from the EU-SMS project, this 70 cm chord A320 prototype is adapted for cruise conditions corresponding to the transonic regime, where the afore mentioned instabilities are developed. The objective is to investigate the morphing concepts able to manipulate the dynamics of the downstream unsteadiness in the separated shear layers and in the wake, able to modify the upstream SBLI as previously discussed, to control these instabilities with emphasis to the attenuation or even suppression of the transonic buffet. The modification of the aerodynamic performances according to this large

parametric study carried out at Reynolds number of 4.5×10^6, Mach number of 0.78 and various angles of attack in the range of (0, 2.4)° are discussed and the final benefits evaluated.

Section 2 presents the physical parameters and the numerical set-up. Section 3 describes in detail the governing equations and turbulence model. The numerical methods, mesh sensitivity and time step sensitivity are presented in section 4. Section 5 highlights the flow dynamics in the non-actuated ("static") case. Section 6 presents the outcomes of the morphing cases by comparing them to the static case and providing detailed discussions explaining the obtained effects. Section 7, presents the final conclusions.

2 Physical parameters

The A320 airfoil's chord is of 70 cm The upstream velocity is 232 m/s, temperature = 221 K, pressure 25224 Pa. The corresponding Reynolds number is 4.5×10^6 and the upstream Mach number M= 0.78. It is worth noticing that there is a scarcity of simulations available in the literature regarding the transonic interaction and the buffet prediction with this Reynolds number order of magnitude. The chosen chord length approximately corresponds to half the A320 wingtip's chord, which measures 1.5 meters.

2.1 Trailing edge vibration and slight deformation

The study encompasses a range of angles of attack (AoA) from 0° to 2.4°, corresponding to cruise conditions. Following consultations with Airbus - France, particular attention is paid to the case of AoA= 1.8°. Under these specific conditions, the SBLI is investigated in detail, especially regarding the appearance of the transonic buffet. A comprehensive analysis of buffet dynamics assumes critical importance in the design, because this phenomenon is responsible for drag increase and furthermore it can trigger amplification of dip-flutter instability, characterized by negative damping. The present investigation involves the exploration of frequencies ranging from 250 Hz to 750 Hz (Table 1). The chosen angles of attack align with the standard cruise speed angles, while the selected frequencies are in accordance with hardware operation of the piezoactuators used in prior research conducted by Tô *et al.* (2019) and Jimenez-Navarro *et al.* (2022) for the transonic Reduced Scale (tRS) prototype of the SMS project of 15 cm chord.

Parameters	Values
Actuation Frequency (f_a) [Hz]	250; 300; 500; 750
Angle of Attack (AoA)	0°; 1.8°; 2.4°

Table 1: Actuation frequencies and angles of attack used in this study.

The trailing edge vibration is associated with a small amplitude, according to a deflection angle $\theta = 1^\circ$ upwards and -1° downwards, therefore providing a flapping semi-amplitude h_p in the range (0.2 - 0.3) mm. Figure 2 shows the trailing edge actuation amplitude. Simultaneously, the trailing edge is subjected to a slight deformation according to a second-order polynomial expression (equation 1), studied by Tô *et al.* (2019).
A schematic illustration of this motion is provided in figure 2.

$$y(x,t) = \left(\frac{2h_p}{3L_p^2}(x - x_p)^2 + \frac{h_p}{3L_p}(x - x_p)\right) sin(2\pi f t) \quad (1)$$

where y is the vertical displacement, x is the chordwise direction, h_p is the semi-amplitude at the trailing edge location x_{TE}, $L_p = 3.5\ cm$ is the actuator length, x_p is the origin of the displacement defined by $x_p = c - L_p$. The trailing edge actuation amplitude $a = 2h_p = 0.6\ mm$. f is the trailing edge actuation frequency.

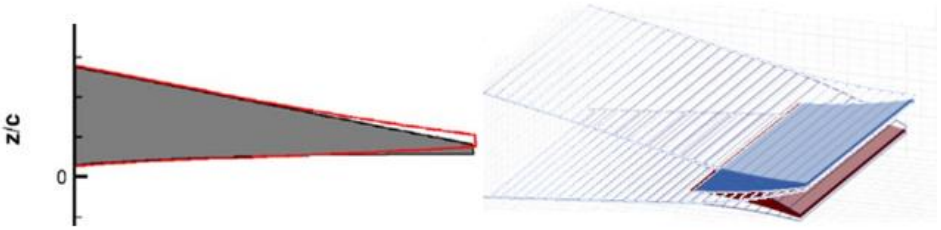

Figure 2: Trailing edge actuation enabling vibration at a constant frequency and amplitude, as well as a slight deformation according to a second-order polynomial.

2.2 Actuation through travelling waves

A more complex morphing concept is examined, as a first step towards creation of a "live-skin" in a specific area of the suction side, through Travelling Waves (TW). The AoA of 1.8° has been considered, as well as two wavelengths, whose first is close to the Kelvin-Helmholtz natural instability wavelength (e.g. in the unactuated – "static" case), along the upper shear layer, evaluated through tracking of these vortices through video visualisations as in fig.7. The vibration frequencies and amplitudes are presented in Table 2 as well as the location and length of the actuation zone, schematically illustrated in Figure 3. The actuation zone begins a bit upstream of the most downstream position of the shock according to the buffet excursion.

Parameters	Values
Amplitude (A) [mm]	0.3; 0.6; 1.2; 1.5
Wavelength (λ) [cm]	3; 6
Actuation frequency [Hz]	250; 500; 750
Actuation zone	30 % of the chord (21 cm)
Angle of Attack (AoA)	1.8°

Table 2: Travelling wave parameters

The travelling wave morphing is modeled numerically with a piecewise function of stationary sinusoidal variation of the "skin" of the lifting structure that produces a travelling wave fluid's motion (equation 2). Figure 3 shows a schematic representation of the travelling waves and their parameters.

$$Z(x,t) = \begin{cases} \frac{x-x_0}{x_1-x_0} A\sin(kx-\omega t+\Phi) & \text{if} \quad x \in [x_0, x_1] \\ A\sin(kx-\omega t+\Phi) & \text{if} \quad x \in [x_1, x_2] \\ \frac{x_f-x}{x_f-x_2} A\sin(kx-\omega t+\Phi) & \text{if} \quad x \in [x_2, x_f] \end{cases} \quad (2)$$

- A is the travelling wave amplitude.
- k is the wave number ($k = \frac{2\pi}{\lambda}$) calculated from the wave length (λ).
- ω is the angular frequency ($\omega = \frac{2\pi}{f_{tw}}$) calculated from the wave frequency (f_{tw}).
- x_0 is the initial coordinate of the piezo-actuator length in the x direction.
- x_1 defines the end of a zone with a linear amplitude increase.
- x_2 defines the beginning of the linear amplitude decrease zone.
- x_f defines the end of the travelling wave zone.

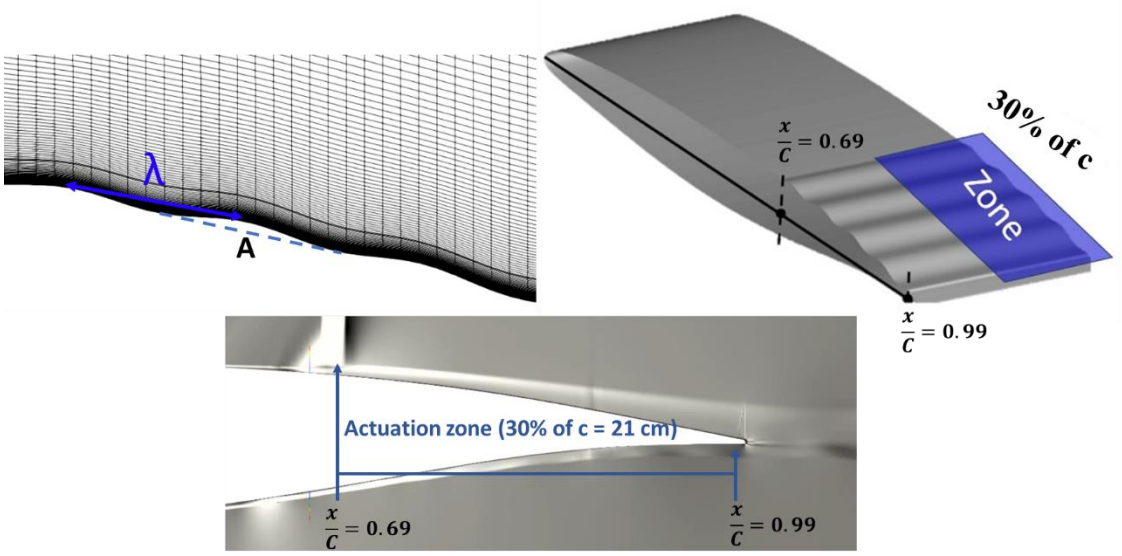

Figure 3: Travelling wave actuation, amplitude, length and zone (30 % of the chord length, 21 cm).

3 Governing equations and turbulence model

The simulations over the A320 aerofoil have been accomplished by using the Navier-Stokes Multi Block (NSMB) code, Hoarau *et al.* (2016), Vos *et al.* (1998). The Navier-Stokes equations are solved for the compressible flow using a specific averaging regarding an adapted turbulence modelling approach, sensitised to capture the coherent structures development as mentioned in the next paragraph. The temporal discretisation used a second order dual time step method (Venkateswaran and Merkle (1995)) and the spacial discretisation for the advection terms used the third order Roe scheme (Roe (1981)) with the MUSCL limiter (van Leer (1979)), as in the study by (Grossi *et al.* (2014)) and (Szubert *et al.* (2015)) for the transonic flow over the OAT15A airfoil. The diffusion terms are discretized according to Jameson's central difference scheme, (Jameson (2007))
The finite volume method is employed on multi-block structured grids, allowing massive parallel computing (MPI). The continuity and momentum equations, according to Favre (Favre (1983)) averaging in respect of the compressibility and in cartesian coordinates are expressed in their conservative form as follows:

$$\frac{\partial \bar{\rho}}{\partial t} + \frac{\partial}{\partial x_i}(\bar{\rho}\tilde{u}_i) = 0 \tag{3}$$

$$\frac{\partial}{\partial t}(\bar{\rho}\tilde{u}_i) + \frac{\partial}{\partial x_j}(\bar{\rho}\tilde{u}_j\tilde{u}_i) = -\frac{\partial \bar{p}}{\partial x_i} + \frac{\partial}{\partial x_j}(\tilde{\tau}_{ij} - \bar{\rho}\widetilde{u_j''u_i''}) \tag{4}$$

$$\frac{\partial}{\partial t}\left(\bar{\rho}\tilde{E} + \frac{\bar{\rho}\widetilde{u_j''u_i''}}{2}\right) + \frac{\partial}{\partial x_j}\left(\bar{\rho}\tilde{u}_j\tilde{H} + \tilde{u}_j\frac{\bar{\rho}\widetilde{u_j''u_i''}}{2}\right) = \frac{\partial[\widetilde{u_i}(\tilde{\tau}_{ij} - \bar{\rho}\widetilde{u_j''u_i''})]}{\partial x_j} + \frac{\partial(\bar{q}_j - \bar{\rho}\widetilde{u_j''H''} + \widetilde{\tau_{ij}u_i''} - \frac{1}{2}\bar{\rho}\widetilde{u_j''u_i''u_i''})}{\partial x_j} \tag{5}$$

Where:

$$\bar{p} = \bar{\rho}r\tilde{T} \text{ and } \widetilde{\rho u_i} = \bar{\rho}\tilde{u}_i. \tag{6}$$

$$t_{ij} = -\bar{\rho}\widetilde{u_j''u_i''} \tag{7}$$

the Favre-averaged Reynolds stress tensor

The turbulent kinetic energy of the turbulent fluctuations: $\bar{\rho}K = \frac{1}{2}\bar{\rho}\widetilde{u_j''u_i''}$ is modelled according to the turbulence modelling approach OES – Organised Eddy Simulation, able to predict correctly the coherent structure dynamics and the related flow instabilities as presented in the following.

Organised Eddy Simulation (OES)

This approach is classified between the statistical (URANS) and LES (Large Eddy Simulation) approaches. It is inspired from groundbreaking experimental studies concerning the coherent structures that began in the middle of the 1970s, including those by Brown and Roshko (1974), Cantwell and Coles (1983) and Hussain and Reynolds (1970), among other. They drew on the highlights of the development of coherent structures in turbulent shear flows, including those around bodies. These studies allowed for the experimental measurement and proper averaging of the underlying structures governing the turbulent shear flows by introducing the phase-averaging, or ensemble-averaging. With the help of this new understanding, it has been demonstrated that turbulence is more than just a chaotic process and has a dual character, with chaotic structures buried within coherent ones. More recent experimental studies in the Institut de Mécanique des Fluides de Toulouse (IMFT), Djeridi *et al.* (2003) including those under the European Research project DESIDER ("Detached Eddy Simulation for Industrial Aerodynamics"), referenced as "The IMFT circular cylinder", Perrin *et al.* (2008), Perrin *et al.* (2007), Haase, Braza and Revell (2009), allowed quantification and distinction of the coherent and chaotic turbulence in the wake past a circular cylinder at high Reynolds number, Braza *et al.* (2006). They provided the basis for the turbulence spectrum splitting approach (figure 4) that regroups the coherent processes under the resolved turbulence and the chaotic ones in the modelled part. Furthermore, the above experiments quantified for the first time in the literature the stress-strain misalignment and the non-equilibrium turbulence spectrum form (fig. 4) that made possible the construction of a tensorial eddy viscosity modelling, Bourguet *et al.* (2008), by projecting the Differential Reynolds Stress Modelling (DRSM) of Gatski and Speziale (1993) on the principal directions of the strain rate. This model solves transport equations for the stress-strain misalignment angle that allows deriving the tensorial eddy-viscosity terms. Furthermore, by employing the DRSM modelling, (Hoarau (2002)), demonstrated that

an equivalent eddy-diffusion coefficient C_μ takes the values in the order of 0.02- 0.03 instead of 0.09 as in the case of equilibrium turbulent flows. These experiments have been widely used for turbulence modelling validation by a considerable number of research institutes, for example in the DESIDER EU project Haase, Braza and Revell (2009).
As mentioned, the OES approach splits the energy spectrum (Fig. 4) into two parts, the coherent motion to be resolved and the chaotic part to be modeled, based on the ensemble (phase) averaging decomposition of the physical variables. Therefore, the criterion to distinguish the resolved turbulence from the modeled one is not the size of the structures as in LES, but their physical character, organised or chaotic. This yields a non-intrinsic 3D character in OES as is the case in LES and hybrid (RANS-LES) approaches, because main physical characteristics of the coherent structures have a 2D origin. Therefore, OES can be used in 2D as a first step, thus permitting accomplishment of large parametric studies as the present one, from which first optimal ranges can be detected and used in more reduced parametric intervals in 3D.

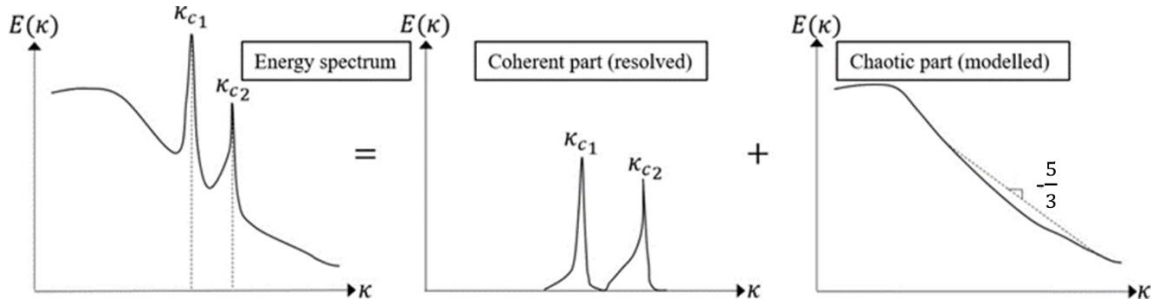

Figure 4: Energy spectrum splitting in OES, from Simiriotis *et al.* (2019).

The present approach has been implemented in the context of the Detached Eddy Simulation, by providing the DDES-OES method, "Delayed Detached Eddy Simulation with embeded Organised Eddy Simulation", where the turbulence length scale in the near wall region has been taken from the OES approach, (Bourguet *et al.* (2008), Marouf et al, (2020)). This allowed taking into account the non-equilibrium turbulence effects in the near region and a smooth passage towards the outer LES region by avoiding Massive Stress Depletion (MST) effects. A view of the performances of this approach is provided in Figure 7, section 5.

4 Numerical method

The computational domain used in this study is $80c$ dimension on each side of the airfoil. A multi-block structured grid M1 with 461K elements (Figure 5, 6 respectively) has been considered and a time step dt2 of 10^{-6} s. This grid and time step were chosen after a detailed sensitivity study, as shown in Tables 3 and 4 respectively. To represent a dynamic deformation and motion of the trailing edge during morphing, the computational domain and geometry are deformed using the Arbitrary Lagrangian-Eulerian (ALE) method of Donea *et al.* (1982).

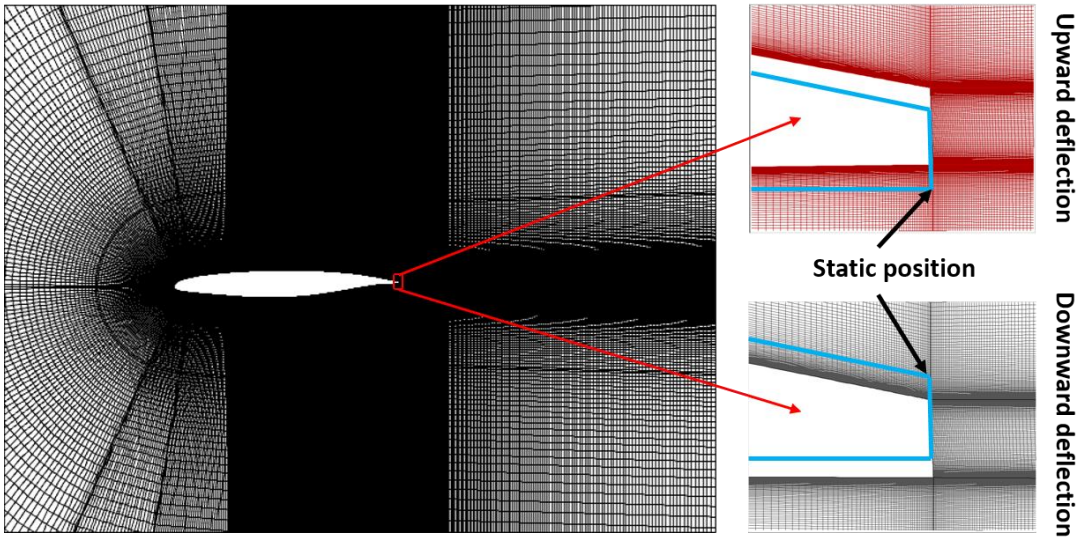

Figure 5: Computational grid over the A320 airfoil, Trailing Edge (TE) deformation.

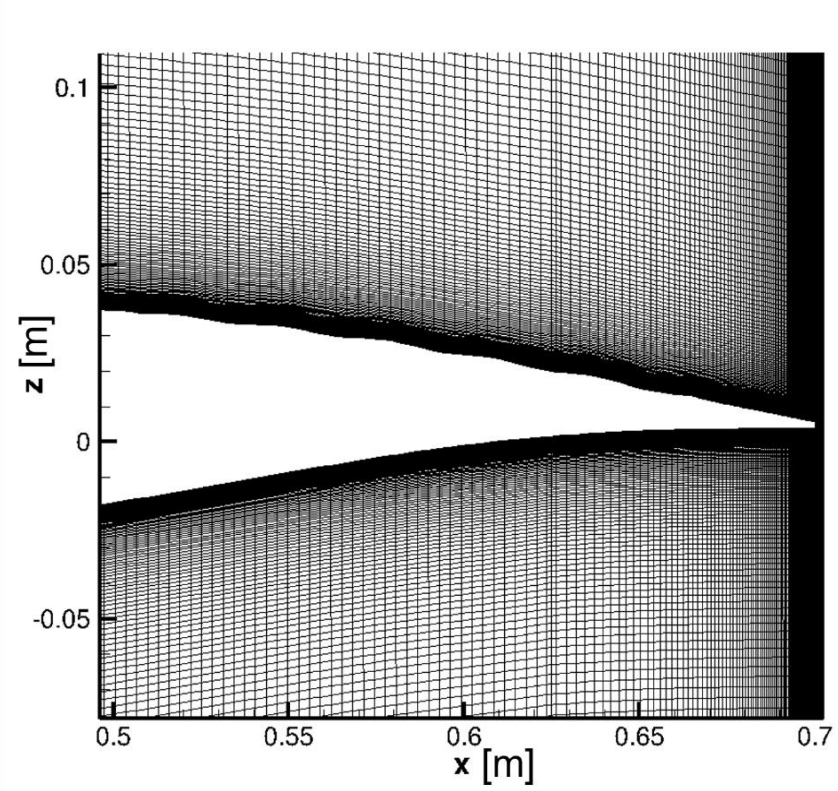

Figure 6: Zoom of the computational grid over the A320 airfoil, Travelling Wave (TW) deformation. In this figure, the vertical axis has been distorted, to allow visualization of the TW on the surface and the near wall mesh.

4.1 Mesh and time sensitivity

The sensitivity of the time step and grid studies are presented in table 3 and 4, respectively. Three different time steps were investigated, and the results showed a relative variation of as little as 0.2 % in comparison to the reference case dt1; dt1 of $0.75e^{-6}$ required more time to converge, thus the present study used dt2 = $1e^{-6}$ as the definitive time step that has little variance when compared to the reference case. In the

context of the mesh study, it has been performed for a more stiff case of 4° AoA characterized by a stronger SBLI and separation impact. the efficiency of two other meshes, M2 with 700,000 elements and M3 with 900,000 elements has been compared to the original mesh. This comparison, once again, highlighted the relative variances regarding the reference cases. Notably, the results revealed relatively minor differences, with lift coefficients varying by an order of 0.2 % and drag coefficients varying as 0.56 % at maximum. The CPU time for the 700,000 and 900,000 element meshes was double the one of reference case. As a result, the M1 mesh of 461,000 elements has been finally adopted.

Time Step [s]	$\overline{C_D}$	$\frac{\overline{C_D} - \overline{C_{D_{ref}}}}{\overline{C_{D_{ref}}}} \times 100$	$\overline{C_L}$	$\frac{\overline{C_L} - \overline{C_{L_{ref}}}}{\overline{C_{L_{ref}}}} \times 100$
dt1(Ref): $0.75e^{-6}$	0.010098	0 %	0.5509	0 %
dt2: $1e^{-6}$	0.010120	0.217 %	0.5525	0.29 %
dt3: $1.25e^{-6}$	0.010117	0.19 %	0.5515	0.11 %

Table 3: Drag and Lift coefficient carried with different time steps sensitivity, 1.8° AoA.

Number of Mesh volumes	$\overline{C_D}$	$\frac{\overline{C_D} - \overline{C_{D_{ref}}}}{\overline{C_{D_{ref}}}} \times 100$	$\overline{C_L}$	$\frac{\overline{C_L} - \overline{C_{L_{ref}}}}{\overline{C_{L_{ref}}}} \times 100$
M1(Ref): 461k	0.0354	0 %	0.6389	0 %
M2: 700k	0.0356	0.56 %	0.6403	0.2 %
M3: 900k	0.0356	0.56 %	0.6403	0.2 %

Table 4: Drag and Lift coefficient carried with different Mesh volumes for AoA of 4°.

5 Flow dynamics in the non actuated case

Figure 7a depicts the three-dimensional flow structure of the unactuated A320 prototype at Re = 2.06×10^6 through illustration of the velocity magnitude iso-contours (red-blue) and the density gradient (grey). Along the suction side and downstream of the SBLI area, counter-rotating shear layer (Kelvin-Helmholtz-KH) vortices are formed with a distinguished organised wavelength being in the order of 3.5 cm, corresponding to ~ (1/20) of the chord. Downstream of the trailing edge these structures are grown and form also a spanwise undulation that results from the amplification of a secondary instability on these primary vortex rows. The interaction between the upper and lower separated shear layers farther downstream in the wake form the von Kármán vortices that also undulate spanwisely with a larger wavelength, as studied in numerous DNS works among which those of the present research group (Braza *et al.* (2001)).

The creation of the coherent vortices after amplification of the instabilities in the separated shear layers past the SBLI and in the near wake thicken the wake as well as the surrounding effective obstacle delimited by the boundary layer and the shear layers and this results in an increase of drag and loss of lift. On each crest of these vortices, secondary shocks develop, due to the local thickening of the effective obstacle and significantly intensify the wave drag.

In two dimensions, the static (unactuated) flow is characterized by the normal shock and its lambda foot, the separated area (blue region) and the formation of KH vortices along

the two separated shear layers with emphasis to the upper one, most affected by the shock's motion (figure 7b). Farther downstream, the interaction between the two shear layers yields the von Kármán alternating vortex shedding.

Thanks to the morphing, as will be shown in this study, a considerable attenuation or even suppression of these instabilities and the associated vortices will be obtained in specific ranges of the vibration parameters considered, yielding a substantial aerodynamic performance increase and simultaneously a reduction of the noise sources produced past the trailing edge. In this study, a comprehensive two-dimensional parametric analysis has been carried out at Reynolds number of 4.5×10^6, that corresponds to the A320 morphing prototype of 70 cm chord. This large parametric study (see Table 1) allows identifying optimal ranges for these parameters, serving as a basis for subsequent Machine Learning approaches used in our ongoing HORIZON-2023-PATHFINDER Project N° 101129952-BEALIVE-"Bioinspired Electroactive multiscale Aeronautical Live skin", allowing for enrichment of the parametric space and application of suitable optimisation approaches. This effort, driven from the present two-dimensional investigation leads also to selected three-dimensional simulations in the detected optimal ranges, to perform more detailed Hi-Fidelity results and to avoid running an impracticable number of 3D Hi-Fi simulations.

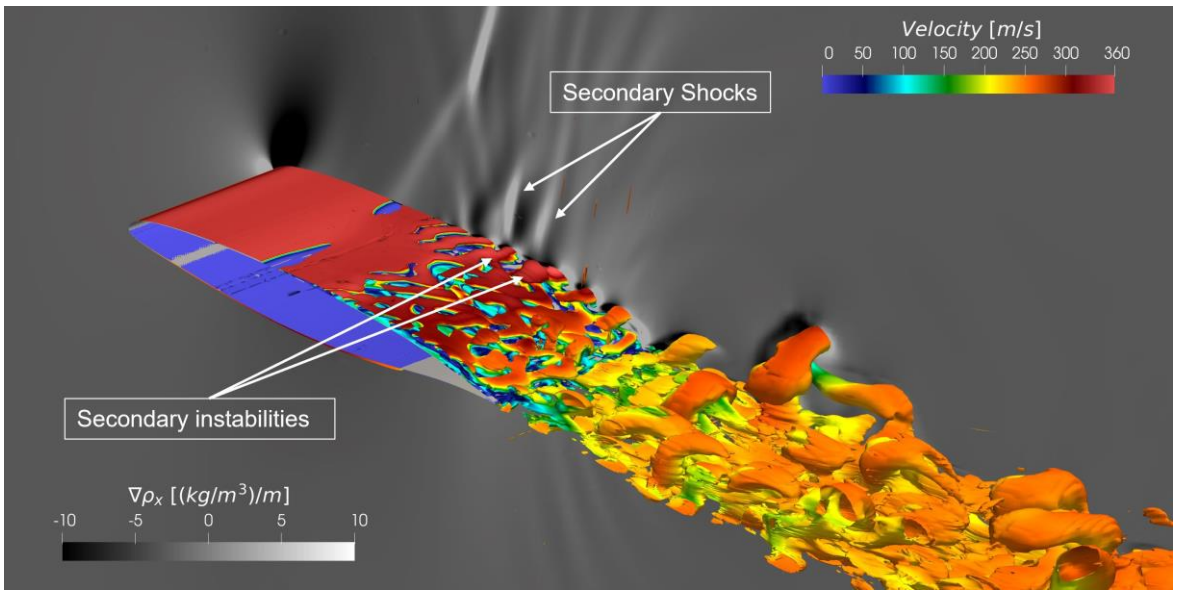

Figure 7a: DDES-OES numerical simulation of the flow around the A320 tRS transonic Reduced Scale prototype of the EU SMS project, Re= 2.06×10^6 (Jimenez-Navarro *et al.* 2022). Q-criterion iso-contours coloured by the velocity magnitude and iso-density gradient iso-contours displayed at the symmetry plane.

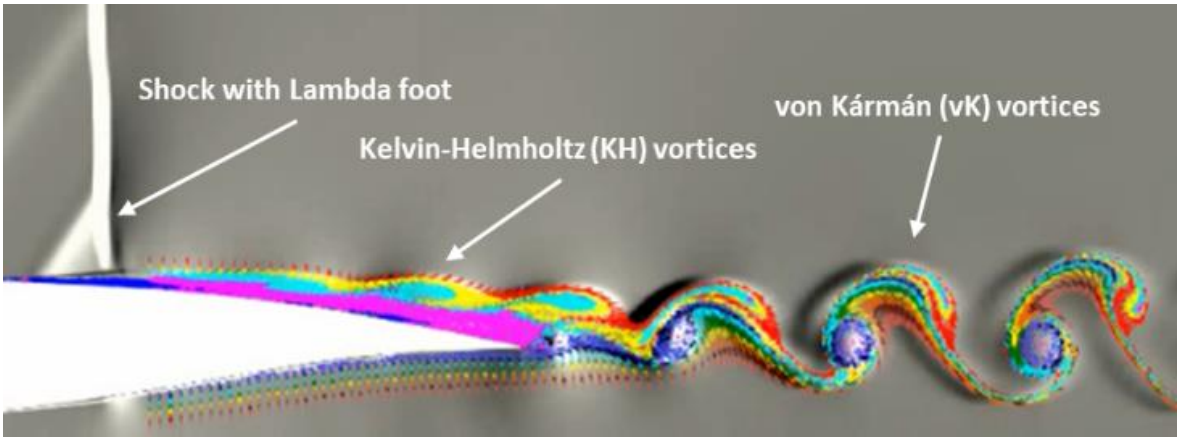

Figure 7b. Coherent structure dynamics in association with the shock-boundary layer interaction area and the flow separation (blue region) through strong feedback effects, Re=4.5M.

6 Results

Prior to investigating the morphing cases, static (non-actuated) case simulations were conducted to obtain the reference flow structure with its natural instabilities and coherent vortices, as well as to evaluate the time-dependent and mean lift and drag coefficients for the purpose of comparison with the morphing cases, according to the two different concepts as explicated in section 2.1 and 2.2.

6.1 Static case at Angle of Attack (AoA) 1.8°

Figure 8 shows two different lift coefficient signal, first signal (Top) for a classic buffet scenario (M=0.78, Re=2.06x10^6) with a 15 cm chord length, creating buffet dynamics with a frequency $f_b = 111\,Hz$, the second signal (Bottom) is the present study, (M=0.78, Re=4.5x10^6) with a 70 cm chord length, a different behaviour is obtained, as shown in this Figure. The lift coefficient displays large "plateau" variations interspersed by decreasing lift intervals. Therefore, two different kinds of shock unsteadiness similar to buffet are observed with buffet frequency $f_{b1} = 6.9\,Hz$ and $f_{b2} = 25\,Hz$ corresponding to two different periods illustrated in this Figure. However, the Strouhal (St) number, ($St=f*c/U_\infty$) for both the classic buffet and the f_{b2} high lift coefficient "plateaus" is equal to 0.07. These are due to the farther downstream movement of the shock wave during longer phases than the ones corresponding to its upstream motion, according to a specific form of the buffet phenomenon in the present case, where the system is trained towards long phases where the shock has moved downstream and stays there over long times. this difference is due to the higher Reynolds number of the present case, comparing to the one on the small prototype. Actually, this situation corresponds to an "attractor" of the present dynamic system towards a reduction of the shock's motion upstream. For even higher Reynolds number, it is plausible that the buffet disappears. This is a case similar to the dynamics obtained for a swept wing, where parts of the span are affected from buffet and parts are not affected, as shown in our previous studies by (Szubert *et al.* (2021)) in the context of the EU - project TFAST.

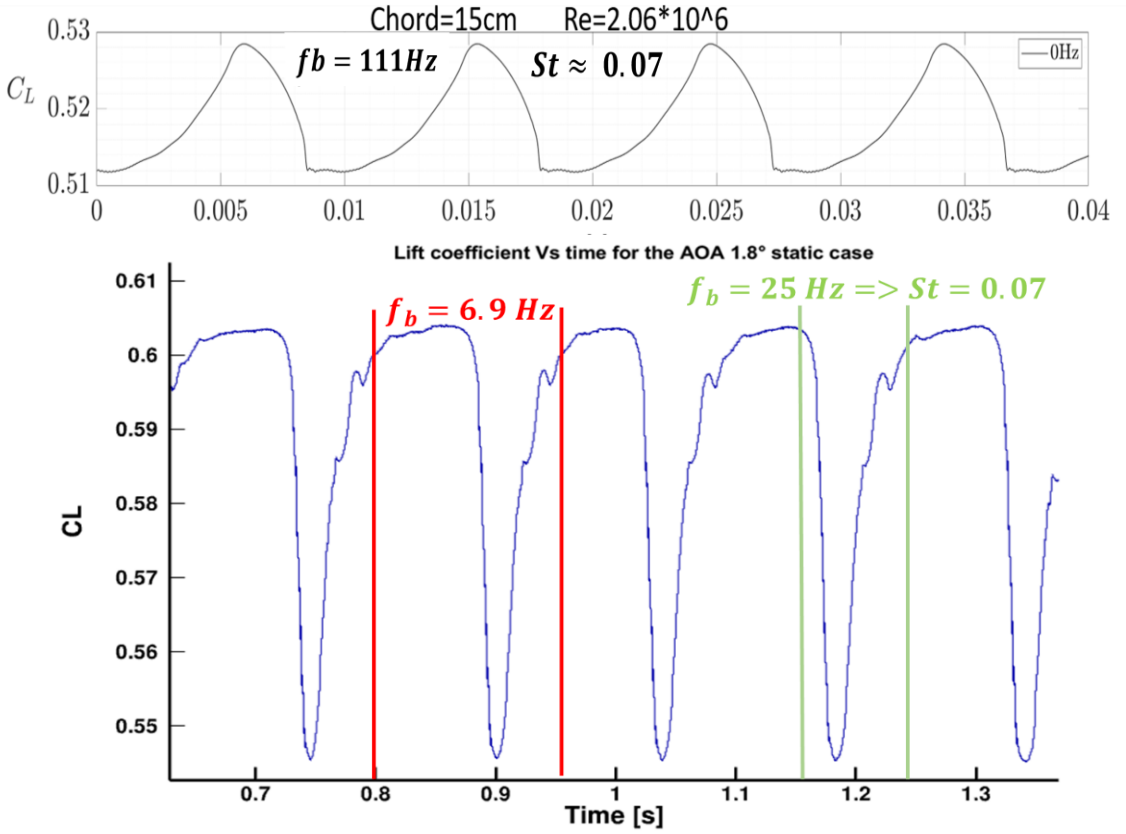

Figure 8: Lift coefficient of the static case: top: classic buffet for AOA 1.8 on 15 cm chord length and Reynolds number Re=2.06 x10^6. Bottom: Buffet with high-lift plateaus, Re=4.5 x10^6.

This "plateau" behaviour and subsequent shorter intervals of lift decrease are further analysed in figure 10 through selected snapshots of the shock and near region vortices motion according to specific videos. The fluctuations in the lift coefficient observed in Figure 8 are a consequence of the shock wave movement on the suction side. This movement occurs due to the interaction of the SBLI area with the downstream instabilities, because under the transonic speeds, the related perturbations can travel upstream of the trailing edge towards the SBLI area. Under the condition that the upstream Mach number is sufficiently high to create strong shear in the supersonic area upstream and on the shock and under the simultaneous action of the downstream unsteadiness, the effect of these perturbations is able to destabilize the upstream (slightly) supersonic area and to lead to amplification of a low frequency instability that is the buffet. It is worth noting that whenever, for any reason, the downstream unsteadiness is attenuated or pushed very downstream from the trailing edge, the buffet is suppressed, as was demonstrated in studies of our research group by introducing a splitter plate downstream of the trailing edge that swept away the non von Kármán mode (Jimenez-Garcia (2012), Szubert *et al.* (2012)).

Although the amplification of the instability in the shearing slightly supersonic region just upstream of the shock can be quantified by, for example, an Orr-Sommerfeld or even a Rayleigh equation, the *reasons for this amplification* are due to *feedback effects* coming from the wake instabilities. The importance of the wake unsteadiness in the mitigation of the buffet had been examined by numerical simulations of Bouhadji and Braza (2003a, 2003b) and Bourdet *et al.* (2003). The above discussed feedback effects, able to

mitigate the buffet instability are precisely employed along the morphing concepts examined in the present study. The widening and narrowing of the near wake and of the shearing regions is caused by the interaction between the shock motion and the shear layer and wake vortex dynamics and visualized in Figure 10. During the phases of the shock motion towards upstream positions, an increase in the thickness of the wake occurs accompanied by a loss of lift as seen on the lift coefficient signal in the low-right corner of Figure 10 where the green line marks the position of the instantaneous snapshot.

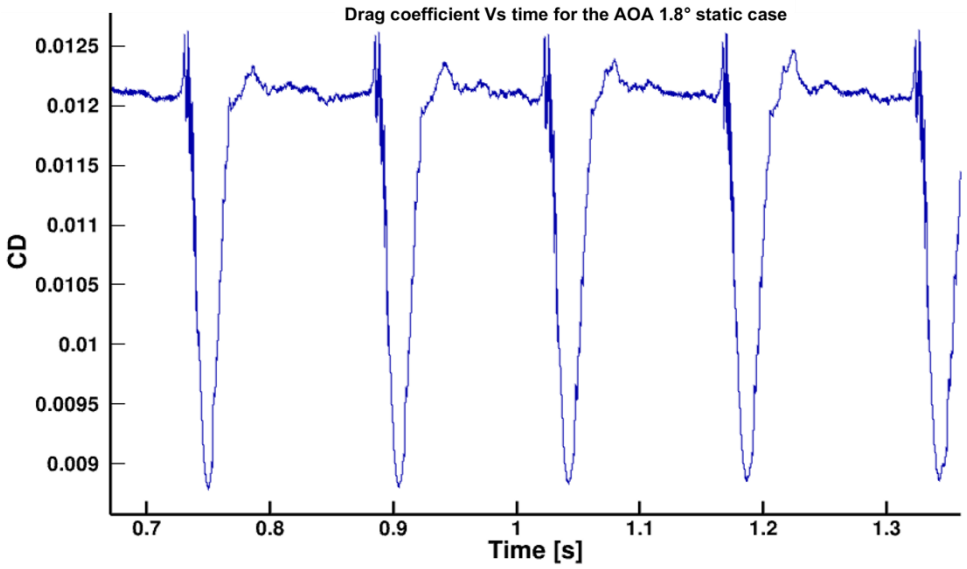

Figure 9: Drag coefficient of the static case results for AoA 1.8° (Re=4.5 ×10^6).

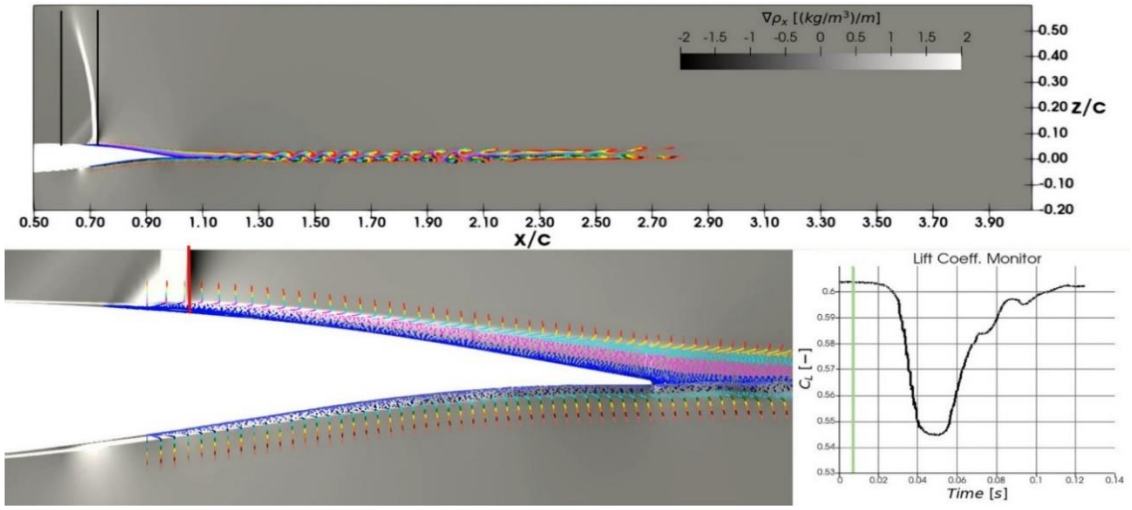

[a]

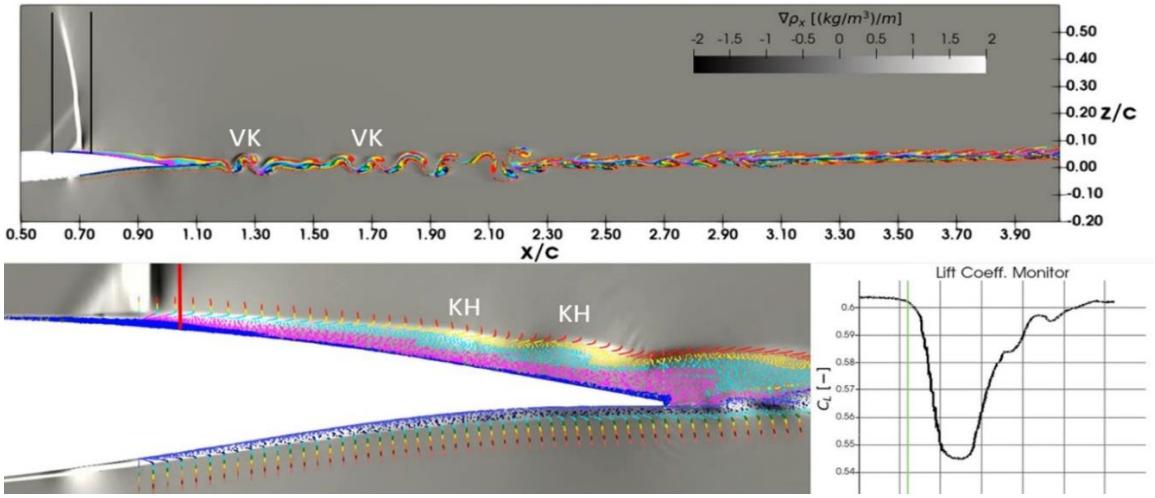

[b]

Figure 10: Static case instantaneous views for AoA 1.8° (Re=4.5×10^6) (a) Instantaneous view corresponding to the high lift plateau phase. (b) instantaneous view corresponding to the phase of lift decrease.

When the lift coefficient is on the plateau (exhibiting a high lift coefficient), it indicates that the wake is relatively thin, devoid of instabilities and the shock wave resides in the maximum downstream position, as illustrated in Figure 10a). Conversely, the reduction in the lift coefficient is attributed to the emergence of Kelvin-Helmholtz and von Kármán instabilities near the trailing edge and in the near wake respectively. These instabilities contribute to the thickening of the wake and the upstream movement of the shock wave, that is pushed considerably away from the red line that denotes the maximum downstream position, (Figure 10b).

6.2 Morphing results

Following the evaluation and analysis of the static cases, the morphing experiments were conducted utilizing two distinct approaches. While the snapshot provided in this paper illustrates the lift coefficient, it is crucial to note that the coefficients of lift and drag are highly correlated, as demonstrated in the static case shown in Figure 8 and 9.

6.2.1 Morphing effects through the Travelling Wave (TW) approach

In the present study this approach focuses on the angle of attack (AOA) of 1.8° and employs three distinct vibration frequencies f_a: 250, 500, and 750Hz. These frequencies are associated with varying amplitudes, wavelengths and zones of application of the travelling wave (TW) along the suction side as was presented in Table 2 and Figure 3.

The travelling waves convection velocity, $Uc = f_a \times \lambda$ is presented in Table 5 as a function of the actuation frequency and the corresponding wavelength. Through tracking the principal coherent eddies in the static case, their shedding frequencies have been evaluated through spectral analysis (Fig. 23 discussed in a next section in comparison with the morphing cases) and their wavelengths estimated from the image processing. The corresponding parameters, as well as their convection velocity are also displayed in Table 5 for the Kelvin-Helmholtz (KH) vortices and the von Kármán (VK) ones. The actuation lambda values employed in this investigation are essential. The von Kármán lambda is in

line with the selection of 0.06, highlighting its applicability. Furthermore, the selection of 0.03 roughly resembles the Kelvin-Helmholtz lambda of 0.035 and correlates to the sub-harmonic of 0.06.

KH (Uc ≈165 m/s and λ = 0.035 m) $f_{KH} = 4714\ Hz$		VK (Uc ≈210 m/s and λ = 0.06 m) $f_{VK} = 3500\ Hz$	
f_a	250 Hz	500 Hz	750 Hz
λ=0.03 m	7.5 m/s	15 m/s	22.5 m/s
λ=0.06 m	15 m/s	30 m/s	45 m/s

Table 5: Convection velocity *Uc* for different Travelling waves, $Uc = f_a \times \lambda$

The convection velocity effect causes an increase of the near wall velocity to change from almost zero to a velocity close to the TW convection velocity, thus reducing the shearing rate that becomes under-critical in respect of this instability amplification that leads to mitigation of the KH vortices and consequent suppression of the buffet in some optimal morphing cases as shown in Figure 12. The blue areas correspond to a TW wavelength of 3cm and the yellow, of 6cm. Figure 11 presents the difference in percentage of the mean drag, lift and lift-to-drag ratio comparing to the static case, according to the different TW applied.

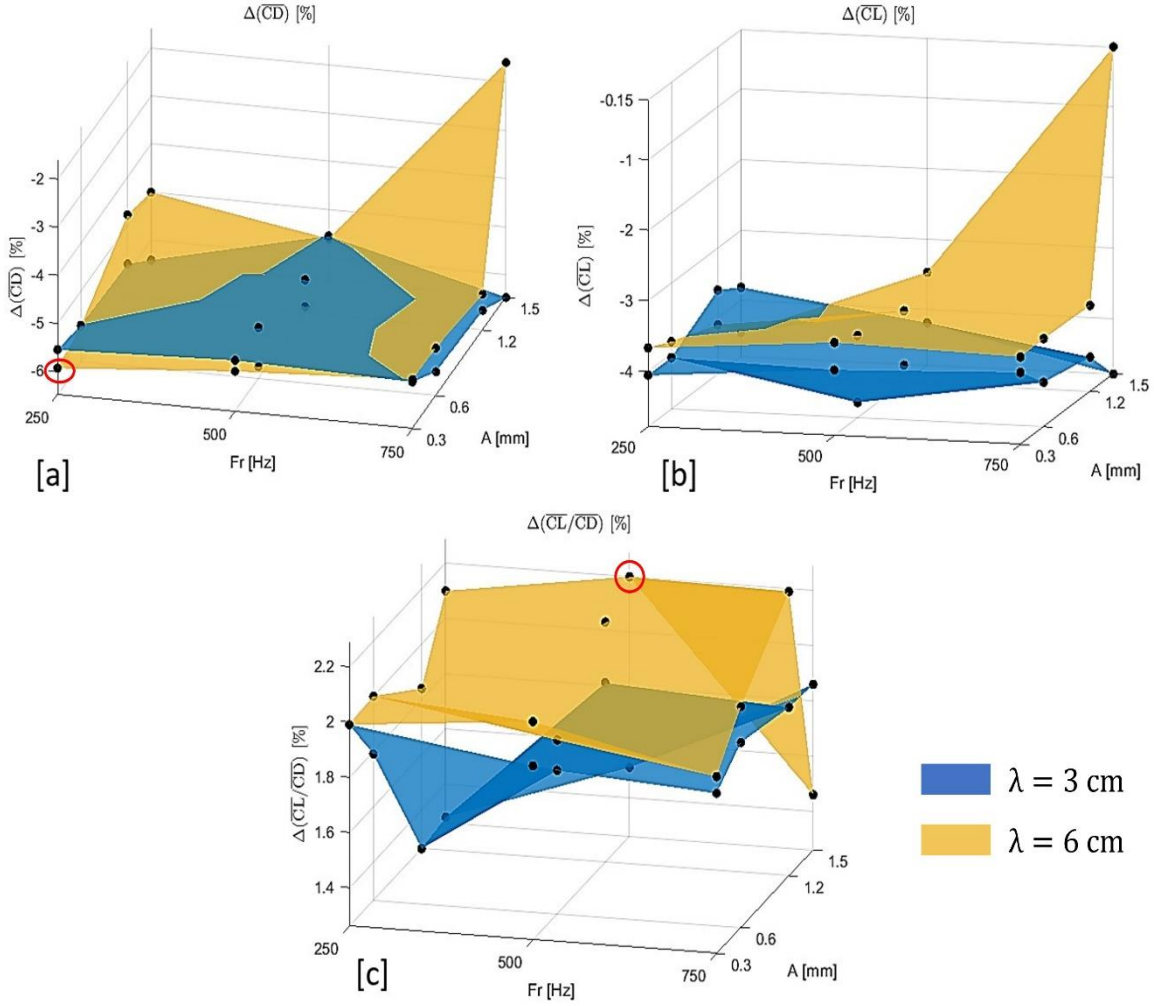

Figure 11: Travelling wave performance results versus actuation frequency and amplitude, in percentage compared to the static case: drag coefficient [a], lift coefficient [b] and lift to drag coefficients ratio [c]. The actuation zone has a length equal to 30 % of the chord, starting from x/c= 0.99 and extends up to x/c= 0.69 (that is slightly upstream of the most downstream position of the shock in the static case) (Fig. 3).

Figure 11(a) shows obtention of a considerable drag reduction in the order of 6 %. The reasons for this good performance are explained in a following paragraph. Figure 11(b) shows no improvement in lift performance. where the best result reaches a slight lift reduction in the order of 0.15 %. This behaviour is related to the actuation zone location of the TW (fig. 3), that was chosen to begin slightly upstream of the most downstream position of the shock foot according to the buffet motion in the static case. The travelling wave actuation increases the blue separated area adjacent to the shock foot (figure 12a), preventing the shock from reaching its maximum downstream position corresponding to the static case (position indicated by the red line). Therefore, the present study indicates an important element: *to start the TW slightly downstream of the most downstream shock excursion*. This study is currently being conducted in the new started European project BEALIVE. It is worth noting in the present case that despite a lack in gain in lift, the drag reduction obtained leads to a significant lift-to-drag increase in the order of 2.2 %, important for the cruise phase of flight that is the most lasting flight phase, leading to a more efficient interaction with the engine and to economy in fuel consumption or more generally to economy in any kind of propulsive energy related to new ones towards zero emissions.

In figure 12a, a considerable thickening of the blue separated area below the shock foot and along the downstream suction side is obtained with a practical mitigation of the KH vortices in case of the actuation frequency of 750 Hz, lambda = 6 cm and amplitude = 1.5 mm.

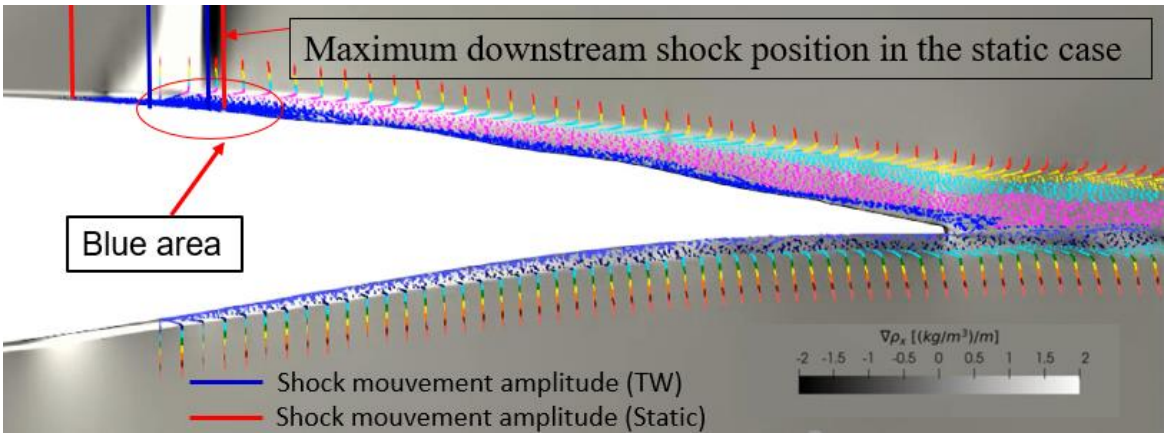

Figure 12a: Suppression of the KH vortices thanks to the TW actuation, f_a= 750 Hz, A = 1.5 mm, λ= 6 cm and actuation zone from x/c=0.99 to x/c=0.69, leading to a "lock-in" of the shock's motion to the actuation frequency. The red vertical line indicates the most downstream shock position according to the buffet in the static case.

The lift coefficient evolution, as well as the density signal located at the shock foot (fig. 13) shows a reminiscence of the buffet frequency *with a short shock's excursion.*

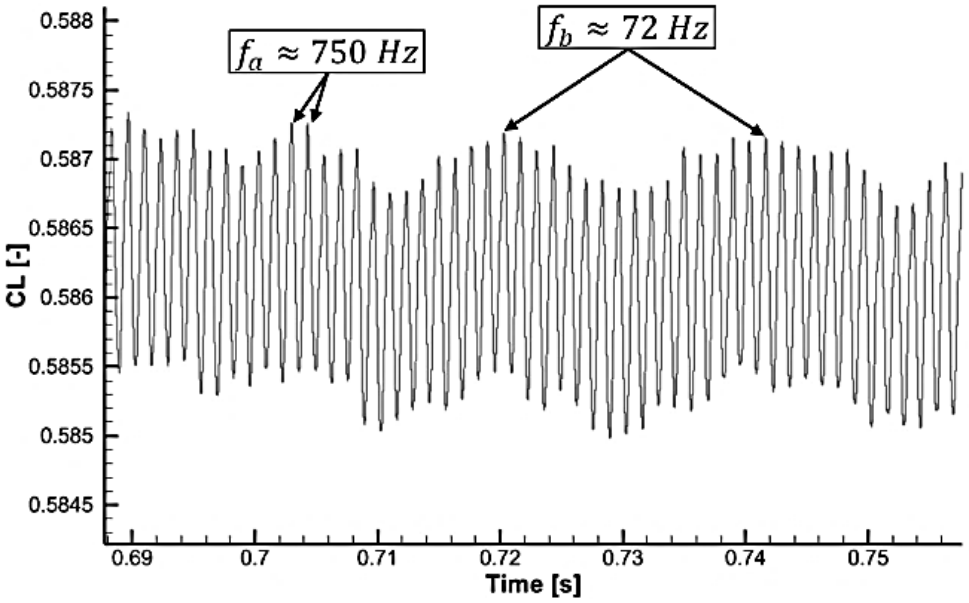

Figure 12b: Lift coefficient versus time, f_a= 750 Hz, A = 1.5 mm and λ= 6 cm.

It is seen that the amplitudes of this reminiscence of buffet are very low. Therefore, the present TW actuation is able to modify the buffet frequency, its amplitude and to reduce the length of the shock' motion in a restricted area in the suction side, close to the position that would take the shock in the static case.

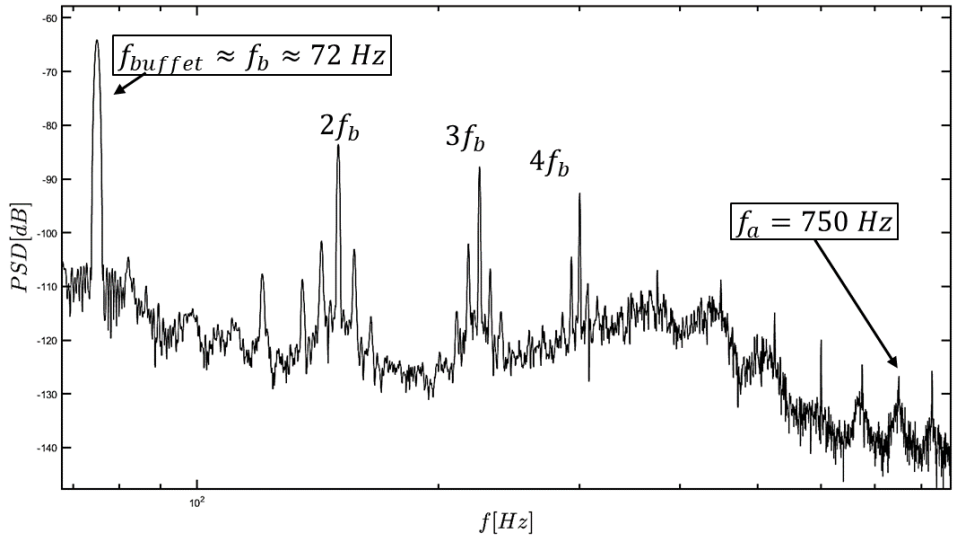

Figure 12c: Power Spectral Density (PSD), Travelling wave with f_a= 750 Hz, A = 1.5 mm and λ= 6 cm.

The system is driven by the reminiscence of classic buffet with a frequency of 72 Hz comparing to the frequency of a classic buffet (fb=111 Hz) at Re=2.06×10^6 (Tô *et al.* (2019)). In the present case, it was shown in the lift coefficient evolution (figure 8) that a successive appearance of lift plateau interspersed from shorter duration decreased lift areas. This periodic occurrence corresponds to a much lower "buffet-like" event whose frequency is assessed through the PSD of figure 13a, but this peak is highly attenuated as shown in this PSD that also indicates a *lock-in* on the actuation frequency of 750 Hz (fig. 13b).

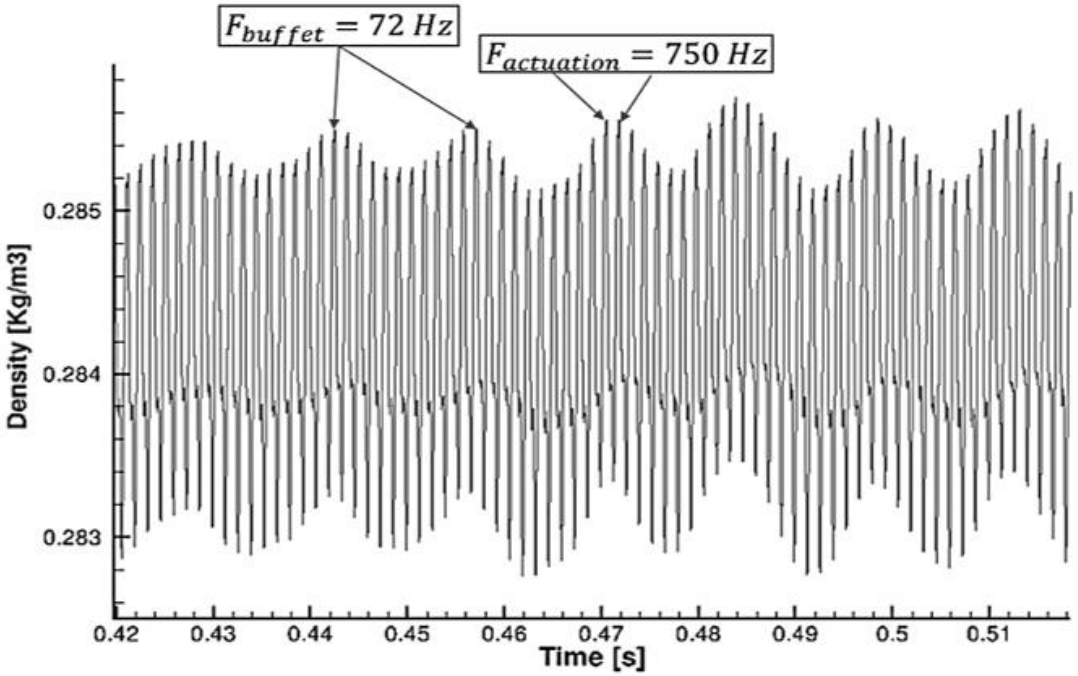

[a]

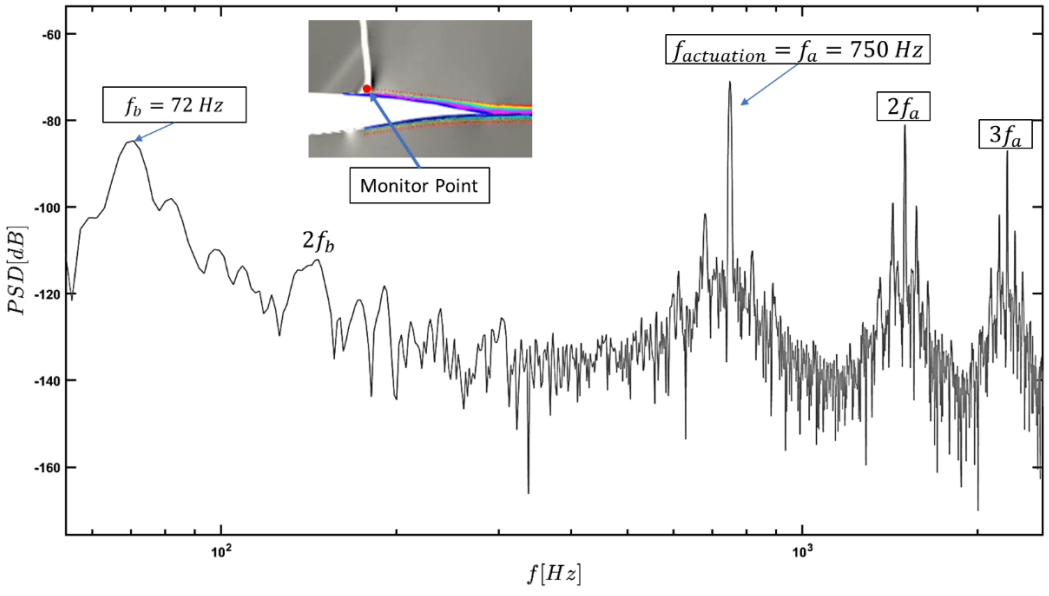

[b]

Figure 13: a) Density variation over time and b) Power Spectral Density (PSD), Travelling wave with f_a= 750 Hz, A = 1.5 mm and λ= 6 cm, presenting the small shock oscillation amplitude using a monitor point placed in the shock wave foot.

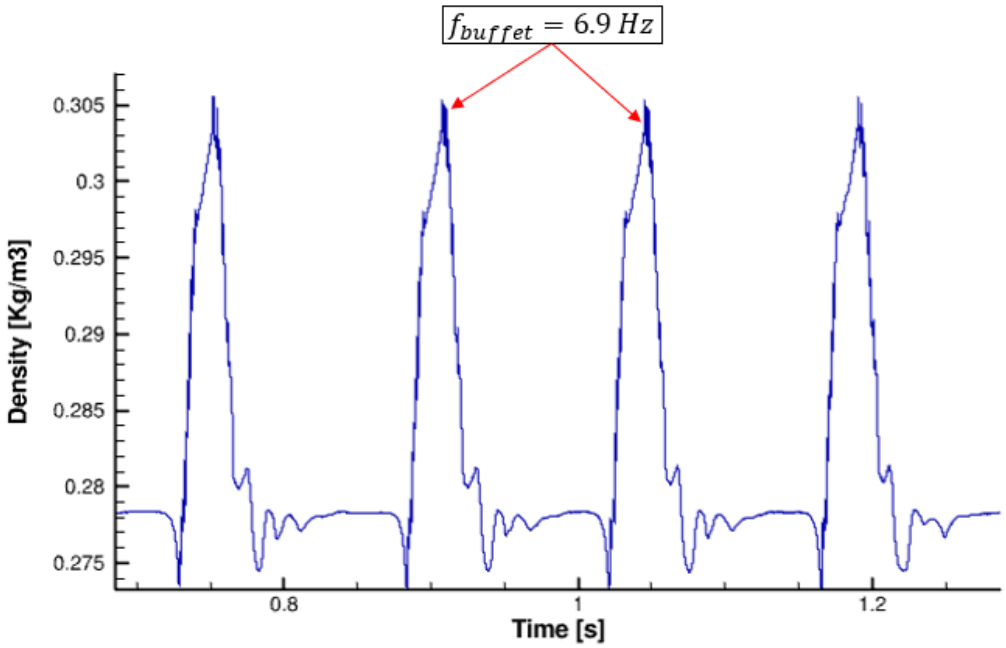

Figure 14: Density variation versus time. The buffet amplitude is much higher than in the actuated case, figure 13(a).

The application of the travelling wave within the boundary layer and the separated shear layer is responsible for increasing air velocity near the airfoil's wall. In figure 15, we can see the air velocity near the wall in the static case is almost zero however by applying the TW approach the velocity increases to 45 m/s. The increase in air velocity within the boundary layer contributes to a shortening of the gap between the boundary layer and upper shear layer with a KH convection velocity approximately equal to 165 m/s having a wavelength of 3.5 cm in the static case. The smaller the shearing rate is, the less development of the KH and VK vortices is, having as a consequence the thinning of the near wake thickness. The KH vortices practically disappear as shown in fig. 12a. This effect prevents the VK vortices to form in the near region. The alternating vortex shedding is swept farther downstream as shown in figure 16 bottom. These facts reduce the wake drag as well as the pressure distribution upstream, thanks to feedback effects previously discussed in section 6.1 third paragraph, thus resulting to a drag reduction as shown in figure 11.

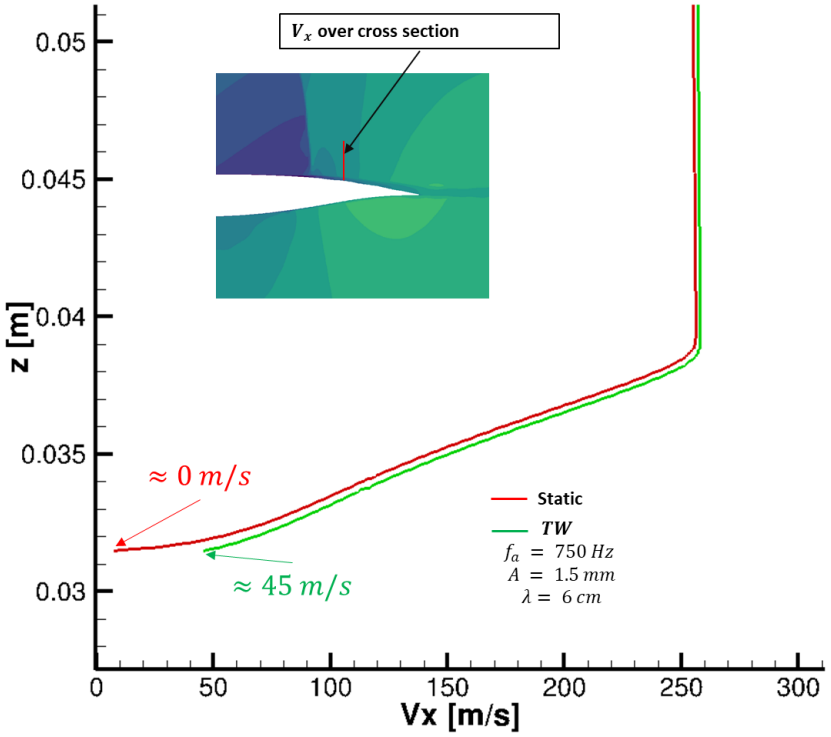

Figure 15: Comparison of the mean (V_x) velocity profiles over a cross-section between static and morphing cases, using the TW approach with f_a= 750 Hz, A = 1.5 mm and λ= 6 cm.

Discussion on the drag reduction mechanism

In Figure 11(a), a significant drag reduction of approximately 6 % is shown in nearly all cases. The explanation for this benefit is as follows: In figure 16, the convection velocity (7.5 m/s) of the TW provides a reduction in the shearing rate comparing to the static case where the near wall velocity is very low. This leads to a practically total mitigation of the shear layer instability and suppression of the KH vortices leading to a considerably thinner near wake's width. Moreover, in this figure it is shown that the shock excursion in the static case is in the x/c range (0.66, 0.72) corresponding to an amplitude of the shock motion of x/c= 0.06, whereas in the morphing case, x/c varies in the range (0.685, 0.718), corresponding to an amplitude of 0.033. This provides a reduction of the shock excursion of 45 %. It is worth noting that in the static case, *the shock amplitude is equal to the lift decrease* and in the morphing case, equal to the amplitude of the sinusoidal variation of the lift. The reduction of the amplitude of the shock motion along the suction side means that the shearing region thickening that accompanies this motion along its upstream phase is shorter than in the static case. Therefore, the shearing region thickness remains thinner during a longer time within the buffet period than in the static case, thus resulting in a reduction in the mean drag. It is also shown that a reduction in the shock amplitude is accompanied by a reduction in the drag and lift oscillation amplitudes. This leads to a reduction of the *rms* of the forces shown in figure 17 that is an additional benefit of the present morphing concept. The unsteadiness due to KH whenever attenuated produces a drastic attenuation of the shock motion.

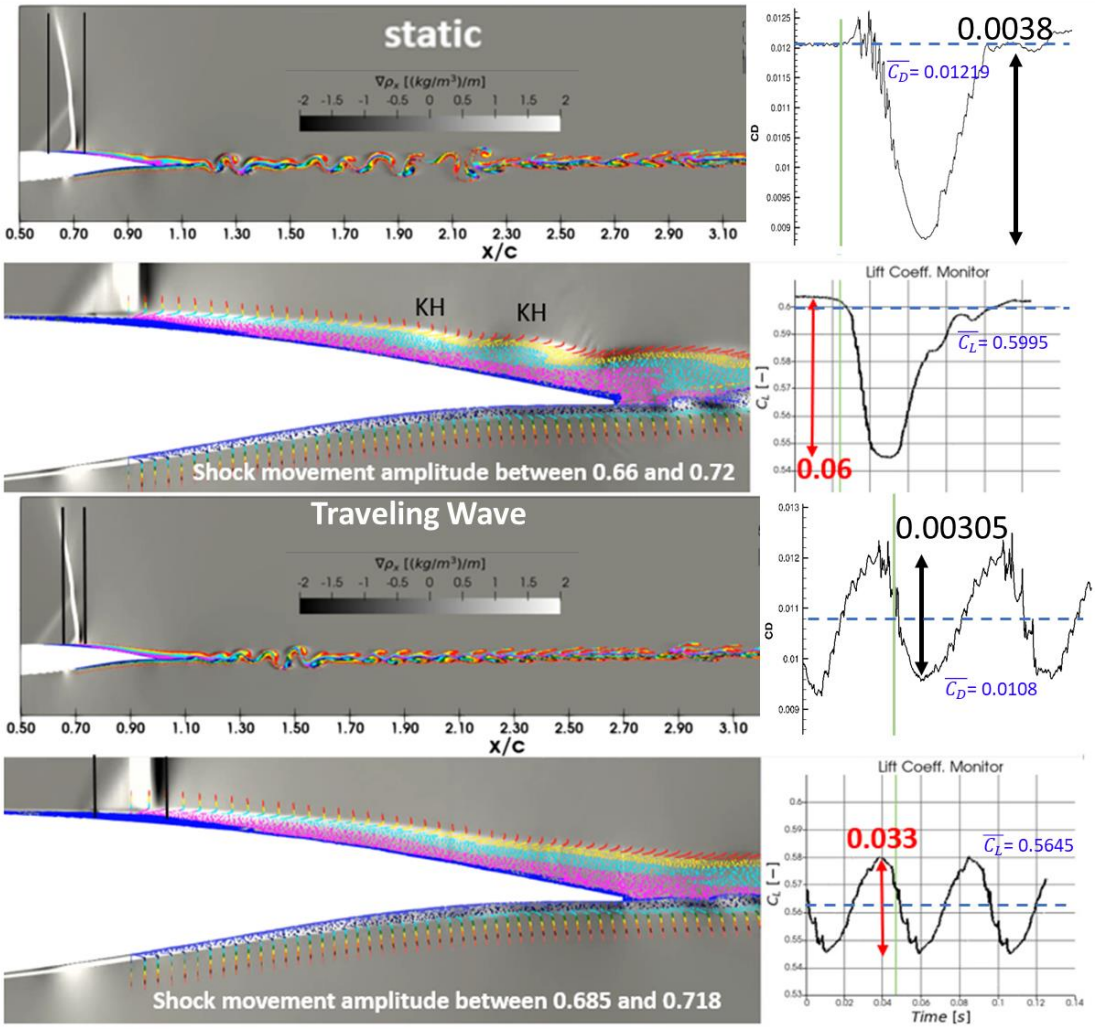

Figure 16: Travelling wave, drag reduction discussion for f_a= 250 Hz, A = 0.3 mm and λ= 3 cm. A decrease of 45 % (0.06 to 0.033) is obtained with an equal decrease of the oscillation's amplitude.

Finally, it is worthwhile noting that the drag reduction (figure 11) occurs in practically all the TW cases investigated, a fact that ensures about a robust morphing concept.

The influence of the travelling wave approach at an angle of attack (AOA) of 1.8° considerably affects the *rms* of the forces, Figure 17 for λ = 3cm and λ = 6 cm. A significant decrease of the *rms* is obtained for both lift and drag. Since the drag force is more sensitive than the lift to the fluctuations, considerable variations are obtained for the $\overline{C_D}'$ in the case of λ = 3 cm and relatively larger actuation amplitudes.
These rms reductions highlight the method's efficiency in stabilizing the aerodynamic performance, emphasizing its potential for improving aircraft stability and control.

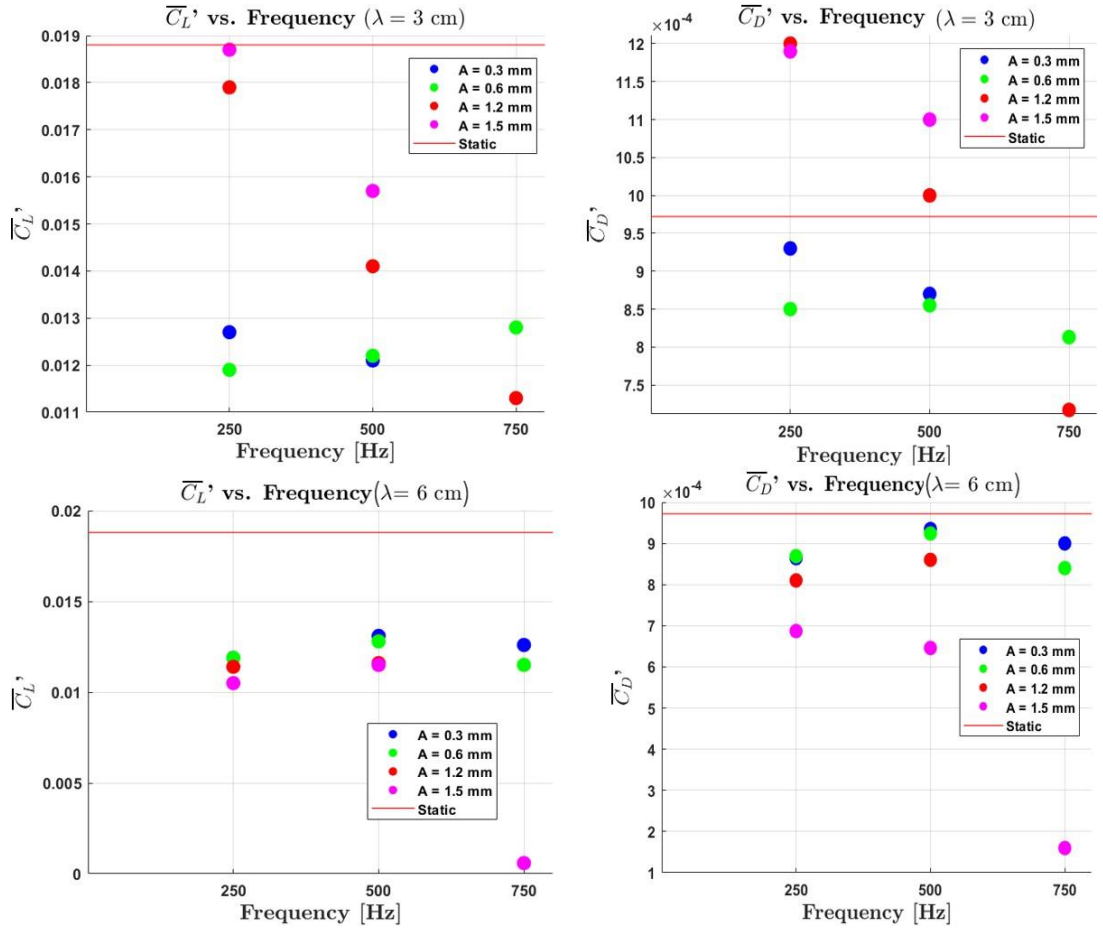

Figure 17: rms of lift and drag, $\overline{C_L}'$and $\overline{C_D}'$, for λ = 3 cm and λ = 6 cm

6.2.2 Trailing edge vibration approach

The present approach concerning the trailing edge actuation, has been previously employed on the so-called "transonic Reduced Scale prototype", tRS of the EU SMS project having 15 cm chord length in the studies by Tô *et al.* (2019) and Jimenez-Navarro *et al.* (2022), corresponding to a Reynolds number of 2.06×10^6, as discussed in section 5. In the present study, the actuation is studied on the 70cm prototype at Mach number 0.78 and Re= 4.5M. From the above previous study, the most interesting actuation frequencies have been considered and applied in the present study, because the Reynolds number range considered corresponds to the same relatively high range, where it is known that the main time and length scales of the coherent vortices governing the dynamic system do not vary in the present range, as studied by numerous examples in the EU-SMS project Braza *et al.* (2023).Therefore, the actuation frequencies considered are in the range of (250,750) Hz, (Tables 6, 7 and 8).

Figure 18 illustrates an example of the signal of the drag coefficient versus time at an angle of attack (AoA) of 1.8° with a 750 Hz frequency of actuation on a 70 cm chord length. The initial irregularity observed at the beginning of the signal in Figure 18 is due to the transient phase of the simulations started by using as initial condition a steady state solution. The influence of the initial condition disappears after a short transient phase. This phase was removed for the evaluation of the mean coefficients as also in case of the previous sections.

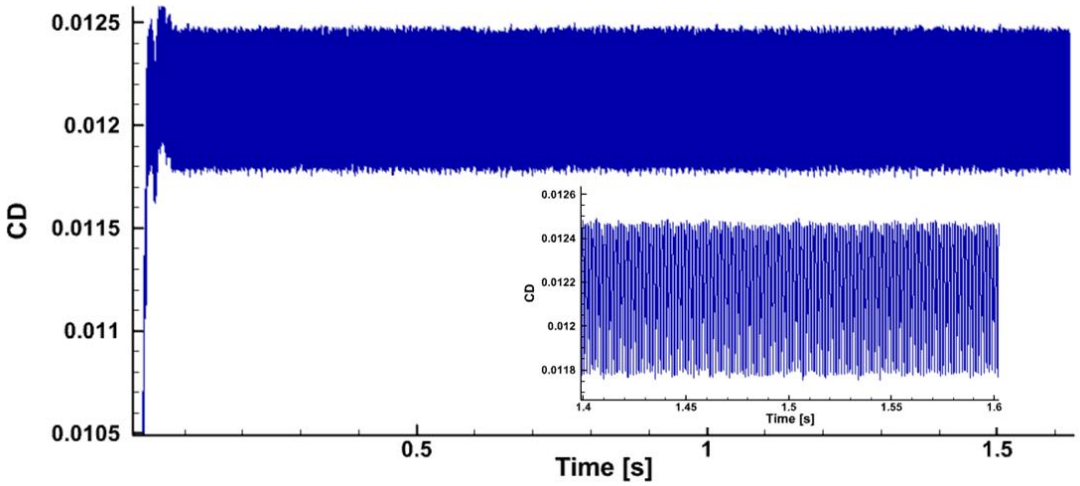

Figure 18: Drag coefficient at 1.8° AoA and 750 Hz frequency of actuation with 0.3 mm amplitude. This evolution shows a "lock-in" of the shock's motion to the actuation frequency and a drastic suppression of the buffet mode shown in Fig. 23

Tables 6, 7 and 8, show the relative modification of the aerodynamic coefficients comparing to the static (non actuated) case. When compared to the static case (Fig. 9), the application of a 750 Hz actuation frequency (Fig. 18) produces a mitigation of the buffet mode and creates a lock-in of the shock motion to the actuation frequency as also shown by Tô *et al.* (2019). This yields a significant improvement in lift *and* drag coefficients as shown in Tables 6, 7 and 8. The highest gains in the performances are depicted by blue colour. It will be remembered that the angle of incidence of 1.8° is the most interesting for the design in cruise conditions, according to interactions of the present research group with AIRBUS, endorser of the EU-BEALIVE project.

Frequency [Hz]	$\frac{\overline{CL}_a - \overline{CL}_{static}}{\overline{CL}_{static}} \times 100$	$\frac{\overline{CD}_a - \overline{CD}_{static}}{\overline{CD}_{static}} \times 100$	$\frac{(\overline{CL}/\overline{CD})_a - (\overline{CL}/\overline{CD})_{static}}{(\overline{CL}/\overline{CD})_{static}} \times 100$
250 (St=0.75)	7.78	-3.66	11.88
300 (St=0.9)	8.15	-2.77	11.23
500 (St=1.5)	10	-1.30	11.45
750 (St=2.26)	10.33	0.25	10.05

Table 6: Relative variation in percentage of the aerodynamic coefficients between static and morphing cases (AoA 0°).

Frequency [Hz]	$\frac{\overline{CL}_a - \overline{CL}_{static}}{\overline{CL}_{static}} \times 100$	$\frac{\overline{CD}_a - \overline{CD}_{static}}{\overline{CD}_{static}} \times 100$	$\frac{(\overline{CL}/\overline{CD})_a - (\overline{CL}/\overline{CD})_{static}}{(\overline{CL}/\overline{CD})_{static}} \times 100$
250 (St=0.75)	-7	-14.13	8.43
300 (St=0.9)	-0.3	-0.64	0.35
500 (St=1.5)	1.65	1.43	0.22
750 (St=2.26)	1.83	0.9	0.75

Table 7 Relative variation in percentage of the aerodynamic coefficients between static and morphing cases (AoA 1.8°).

Frequency [Hz]	$\frac{\overline{CL}_a - \overline{CL}_{static}}{\overline{CL}_{static}} \times 100$	$\frac{\overline{CD}_a - \overline{CD}_{static}}{\overline{CD}_{static}} \times 100$	$\frac{(\overline{CL}/\overline{CD})_a - (\overline{CL}/\overline{CD})_{static}}{(\overline{CL}/\overline{CD})_{static}} \times 100$
250 (St=0.75)	2.45	6.7	-2.97
300 (St=0.9)	0.2	-0.62	0.1
500 (St=1.5)	0.05	-1.2	1.2
750 (St=2.26)	0.5	-0.3	0.24

Table 8: Relative variation in percentage of the aerodynamic coefficients between static and morphing cases (AoA 2.4°).

It is worth noting that achieving simultaneous improvements in lift and drag coefficients obtained in this study, is relatively rare in the state of the art.

For the angle of attack (AoA) of 0°, the results indicate significant gains in lift for practically all the actuations and maximum ones (in the order of 10 %) for the actuation frequencies of 500 and 750 Hz. A drag reduction is also obtained for the actuations of 250, 500 and 750 Hz with a maximum reduction at 250 Hz. The overall aerodynamic efficiency, (mean lift-to-drag ratio), shows a substantial increase for all actuations with a maximum value of 11.88 % at the frequency of 250 Hz, where the most significant drag reduction of -3.66 % is attained.

Concerning the AoA of 1.8°, (Table 7) that highly interests the design in cruise phase, an increase in the lift coefficient for the 500 Hz and 750 Hz frequencies, by 1.65 % and 1.83 %, respectively is obtained. Simultaneously, there is a *significant drag reduction in the order of 14 %* at the frequency of 250 Hz and less for the 300 Hz case. Consequently, an 8.43 % lift-to-drag increase is obtained due to this drag improvement.

The morphing at AoA of 2.4° shows a lift increase of 2.45 % for the case of 250 Hz and less, but positive for the other cases. A maximum drag reduction of 1.2 % has been obtained in the case of 500 Hz. demonstrates its effectiveness in reducing flow instability, even at an angle of incidence of 2.4°, providing an aerodynamic efficiency increase of 1.2 %.

Figure 19 shows simultaneously the mean values of the aerodynamic coefficients as a function of the actuation frequency, as well as the *rms* of the forces for the AoA of 1.8°. The optimal ranges are those satisfying simultaneously a lift increase or drag reduction and a low *rms*. Figure 19a shows that increasing the frequency yields better results in total improvement concerning the lift coefficient with an optimal area around the 750 Hz. This actuation suppresses the buffet excursion as will be detailed in a following paragraph and produces a very short amplitude of the shock's motion that is "locked – in" at this actuation frequency. Concerning the drag (figure 19b), the optimal ranges are those characterized by a drag reduction and simultaneously by a low *rms*. This range is located near the actuation of 250 Hz and is suitable for the take-off flight phase. However, in the last phase of landing, the drag reduction is no more needed because the airplane's speed has to be drastically reduced, but the lift has to be highly increased in this phase to ensure a high lift-to-drag ratio. Therefore, the optimal range for this phase would be around the actuation of 250 Hz as shown in the L/D diagram of figure 19c but also near 750 Hz, where the *rms* of both the lift and drag coefficients is very low.

Therefore, the overall relative optimal areas are indicatively located around the frequencies around 250 Hz and 750 Hz according to the present figures.

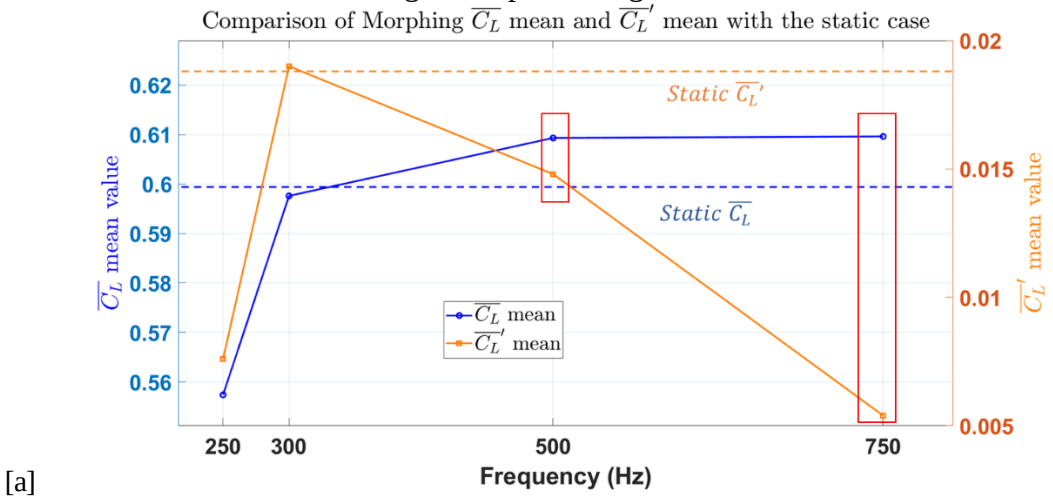

[a]

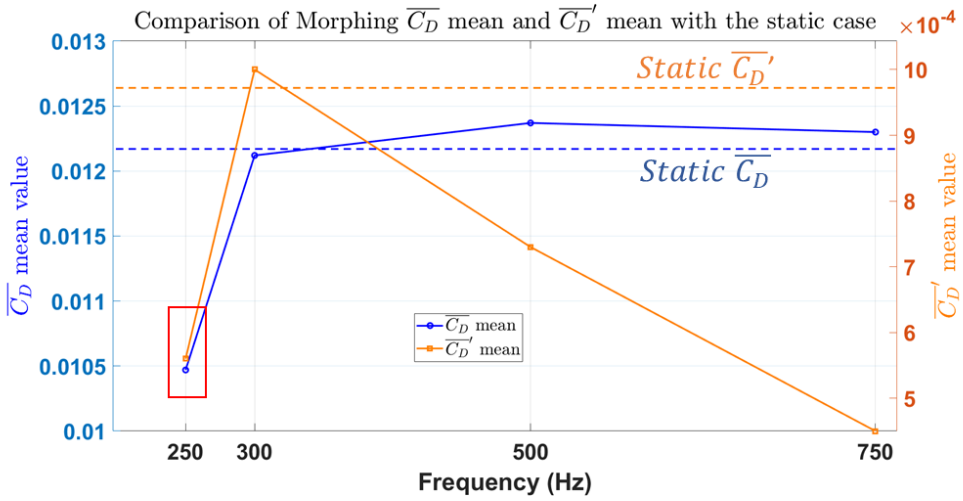

[b]

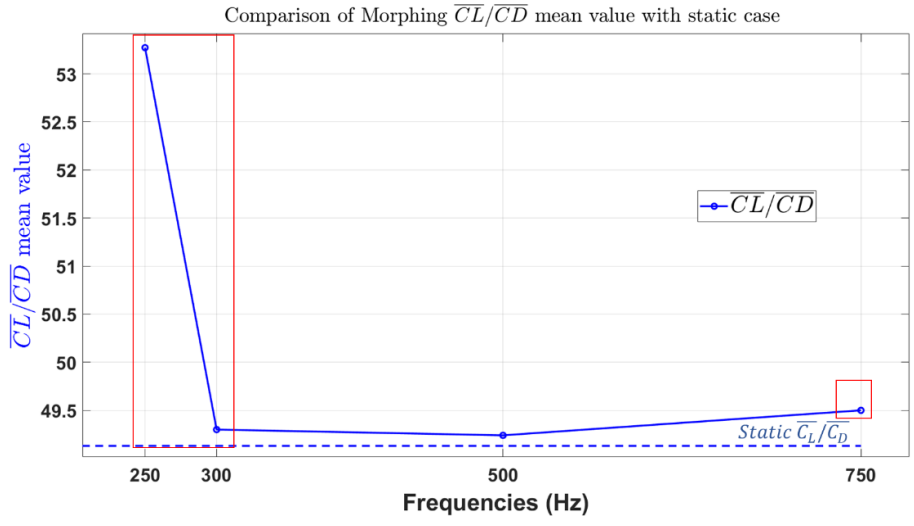

[c]

Figure 19: Evolution of the aerodynamic coefficients and their *rms* (a,b) and of the lift-to-drag ratio (c), as a function of the actuation frequency for AoA of 1.8°.

6.3 Discussion of lift increase, drag reduction and buffet suppression

In this section, two different analyses are presented showing an increase in lift and a reduction in drag. The first case focuses on the average wall pressure coefficient study around the airfoil, while the second examines the *rms* pressure distribution across the shock wave. Moreover, the mechanisms leading to mitigation of buffet and the lock-in mechanism to the actuation frequency are discussed through spectral analysis.

Lift increase

As shown in figure 20, the trailing-edge morphing approach successfully shifted the averaged shock position downstream, resulting in an increase of lift shown in Table 7. This shift in the shock position is accompanied by modifications in the dynamics near the trailing edge and in the wake farther downstream, effectively pushing the von Kármán vortices away from the near wake (Fig. 22(b)). These alterations lead to a thinner wake and allow the shock reaching a maximum downstream position located more downstream than in the static case.

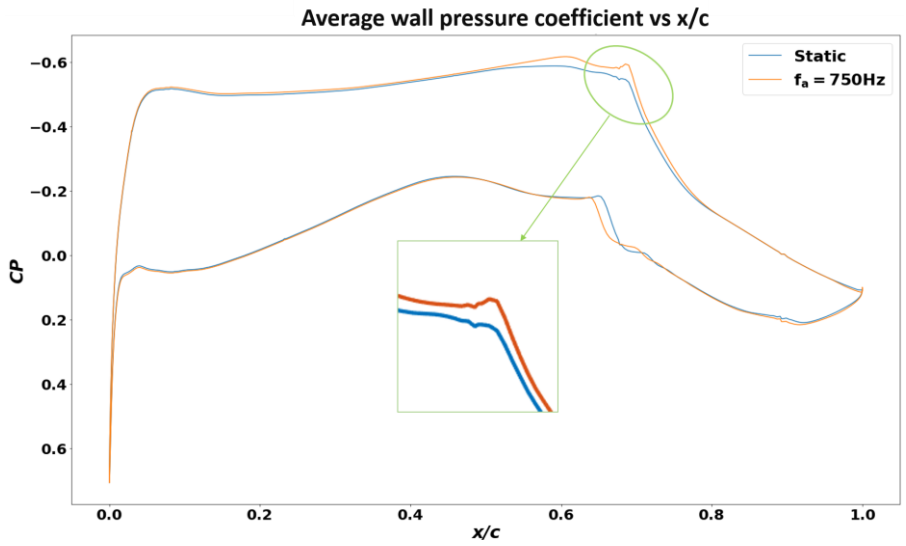

Figure 20: Averaged wall pressure coefficient for the static and morphing cases, AoA of 1.8°.

Drag reduction

The drag experienced by an aircraft's wing is closely related to the strength of the shock wave fluctuation due to the buffet (e.g. the *rms* of the pressure along the wall) and the thickness of the separated area and the corresponding shear layers that it creates. The shape of moving objects in the airflow is influenced by the thickness of the wake they encounter. Thinner wakes lead to thinner shape of the effective obstacle (that is not the nominal profile's shape in this case but the one contoured by the boundary layer and shear layers), which in turn reduce drag. Moreover, in the present transonic regime, thinner separated area and shear layers produce by means of feedback effect an attenuation of the shock's excursion as discussed in previous section with attenuation of the buffet and therefore of the drag. These facts will be shown in the following.

In this study, an "eddy blocking effect" (Szubert *et al.* (2015), (Da Silva, Hunt *et al.* (2014), Hunt *et al.* (2008)), induced by the trailing-edge vibration is obtained (Fig. 22(b)), which produces a shear layer thinning and a sweep of the von Kármán vortices much farther downstream, thus reducing the wake's width. Additionally, regarding the

shock wave's fluctuating motion, the feedback effect resulting from this behaviour contributes to a reduction of the *rms* of the near wall pressure along the shock area (Figure 21). This means that the shock wave reduces its fluctuating excursion along the suction side than in the static case. It has been also seen (figure 20), that it moves in more downstream positions. These effects produce a separated region thinning more intensely than in the static case, leading to the shear layers and near wake thinning and therefore to a consequent drag reduction, *that was evaluated in the order of* ***14 %*** for the AoA=1.8° (Table 7).

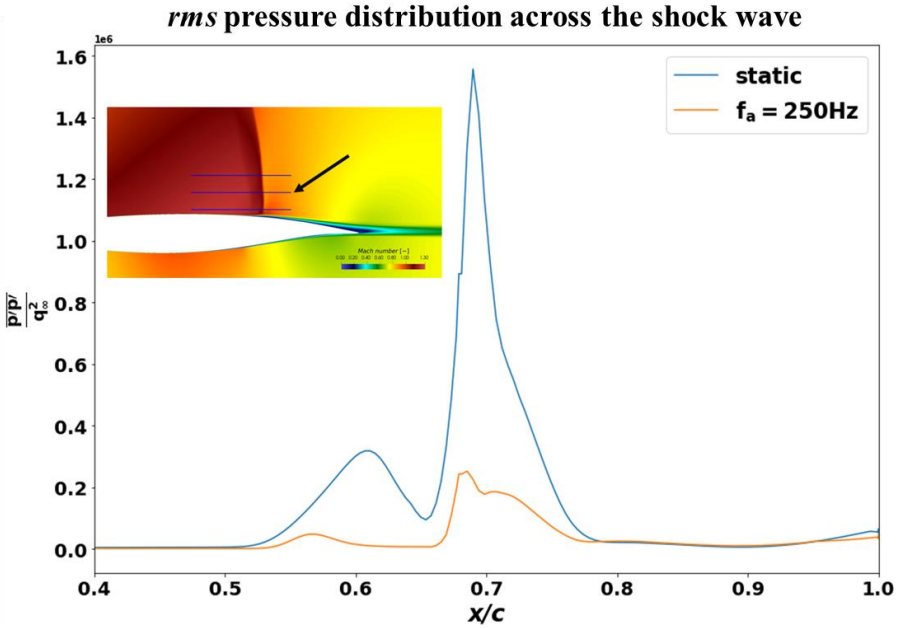

Figure 21: *rms* pressure distribution across the shock wave, along a horizontal line at y/c= 0.125, AoA=1.8°.

Buffet mitigation and lock-in mechanism

Figure 22(a) corresponds to the evolution of streaklines in the static case. Figure 22(b) shows the reduction of the shock's amplitude along the suction side according to lock-in to the actuation frequency of 750 Hz. The lock-in is presented in Fig 23, through the PSD of the pressure signal at a monitoring point in the near wake *x/c, y/c= (1.233,0)* for both the static and morphing cases. This figure shows that the von Kármán frequency bump, occurring in the range (3000, 5000) Hz, is effectively reduced in amplitude and is interspersed by the actuation frequency harmonics, where the main shock's motion is locked-in at the actuation frequency of 750 Hz. The overall PSD in the morphing case, as well as the frequency peaks and bumps obtained, are all characterized by a lower amplitude. The spectral energy reduction occurring thanks to the morphing is around 55 %. This corresponds to a reduction of the noise sources produced by the trailing edge.

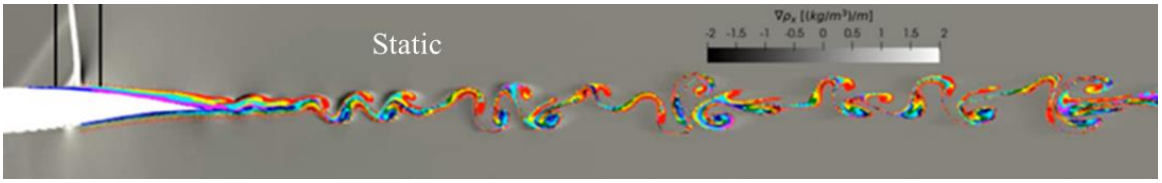

[a]

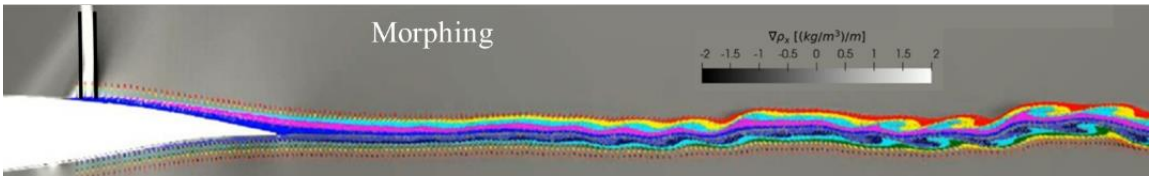

[b]

Figure 22: Streaklines showing the separation, shear layers and coherent vortices, as well as density gradient iso-contours (grey): a) Static case b) Morphing with trailing edge vibration at 750 Hz and amplitude of $a = 2h_p = 0.6\ mm$ illustrating the considerable attenuation of the shear layer vortices and the "sweep" of the von Kármán alternating vortices much farther downstream. The vertical black lines show the area of the shock's motion amplitude. In case [b], a buffet's practical suppression is shown according to the "lock-in", mechanism in respect of the actuation frequency, shown also in the following figure through the PSD of a pressure signal in the near wake.

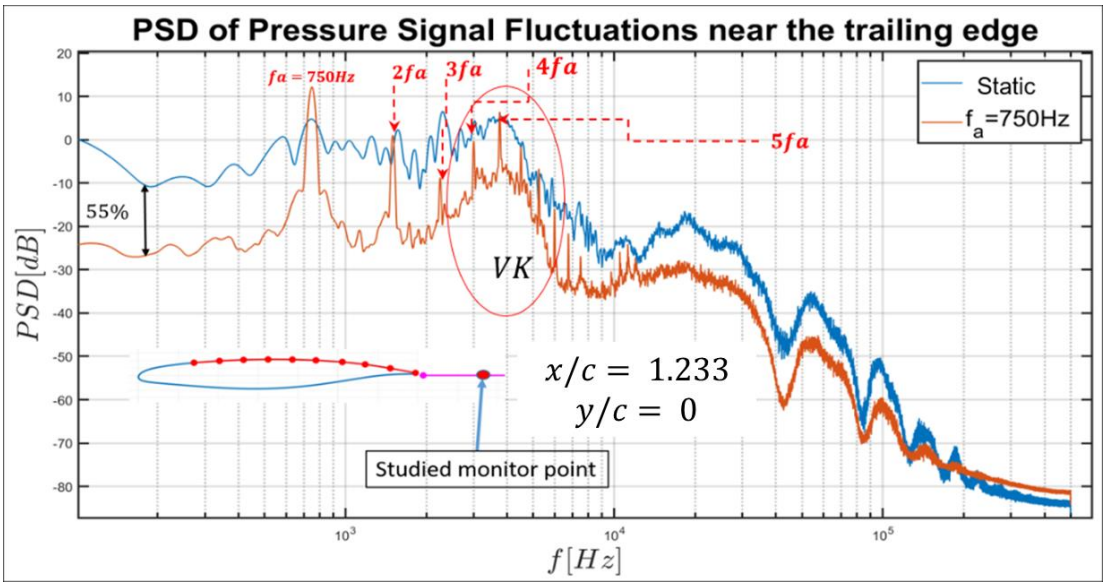

Figure 23: Power Spectral Density (PSD) in dB of the pressure signal at the monitor point *x/c, y/c= (1.233,0)* in the wake, showing a considerable reduction of the overall spectral amplitude, especially in the low frequency range and appearance of the actuation frequency and its harmonics as the only predominant peaks. Considerable attenuation of the frequency bump (blue curve – static case) in the range of (3000,5000) corresponding to the von Kármán vortex shedding thanks to interaction of the actuation frequency harmonics with this frequency bump area, interspersed by these harmonics in the morphing case (orange-brown curve).

The high performances obtained through the mitigation of the buffet phenomenon at the present actuation frequency are also illustrated in the polar curve (Fig. 24), where the blue point corresponding to this frequency shows a maximum performance.
According to a flight mechanics approach used in the EU-SMS project (Farges and Chaboud (2023)), a fuel consumption assessment has been made through a modelled A320 aircraft trajectory in cruise, by using the polars calculated in the present study, indicating a reduction in the order of 3.5 % for the present range of actuation frequencies presented in Table 1. From the European Commission DG MOVE/ DG RTD, Flightpath 2050 report (DG MOVE, 2012), as well as from the ACARE – "Advisory Council for Aviation Research and Innovation" (https://www.acare4europe.org/acare-goals/), it is known that a reduction of fuel

consumption of 1 % is estimated to decrease the average daily CO_2 emissions by 0,030 billion kg and SO_X by 0,1 thousand kg indicatively. This emphasizes the impact of the present morphing concepts towards a cleaner environment in Horizon 2030.

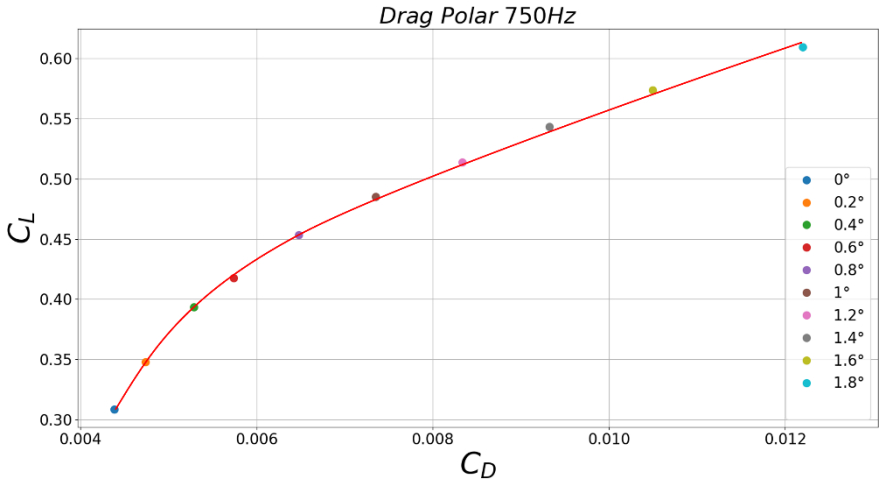

Figure 24: Lift versus drag evolution (drag polar) obtained for the actuation frequency of 750 Hz for different angles of incidence varying from 0° to 1.8°.

7 Conclusion

The present study investigated the transonic flow dynamics and their modification through specific morphing concepts around an A320 airfoil of 70cm chord, at a Reynolds number of 4.5×10^6, Mach number of 0.78 and at angles of attack (AoA) of 0°, 1.8° and 2.4°. The interaction of the shock wave with the near region flow instabilities has been analysed, as well as their influence on the buffet phenomenon. In the present case, the buffet exhibits a different kind of dynamics than the more "classic" one displaying an almost sinusoidal motion. The present buffet makes appearing large "plateaus" of high lift followed periodically by drops of lift. In respect of the present Reynolds number, higher than the 2-to 3 M range where a number of experimental and numerical studies mentioned in the introduction depicted a "classic" sinusoidal-like buffet. The present corresponds to a case "attracted" by dynamics having the tendency to be in-between "non-buffet" intervals, interspersed by "buffet-like" shorter intervals. Two different morphing concepts have been examined in continuation of the studies accomplished through the European research project H2020 N° 723402 "SMS" – "Smart morphing and Sensing for aeronautical configurations", (Braza *et al.* (2023)) around a smaller A320 morphing prototype of 15 cm chord and Reynolds number of 2.06×10^6 actuation along specific areas of the suction side by applying Travelling Waves (TW) of low amplitudes in the order of 1mm and having wavelengths comparable to the separated shear layer instabilities, as well as vibrations and slight deformation of the near Trailing Edge (TE) region. These actuations are realizable by the hardware, through electrical piezoactuators on real A320 wing prototypes with the afore mentioned chord length in a companion study that is underging in parallel with the present simulations, under the French ANR – "Agence Nationale de Recherche" project EMBIA – "Electroactive Multiscale Bioinspired Interfaces in Aeronautics", https://anr.fr/Project-ANR-21-CE05-0006
In respect of this project, the present study had the objective to investigate efficient morphing concepts regarding dimensions closer to the real configurations and to

investigate a first schematic approach towards formation of a "live-skin" along strategic areas of the wing, composed of a high number of novel electrical actuators offering a high DoF feedback controller system.

In both kinds of the morphing concepts investigated (TW and TE actuations), the influence of a fundamental mechanism, the *eddy blocking effect*, able to constrict the shear layers, to reduce the separation area and the near wake's width has been shown regarding the modification of near wake the coherent structures and its strong influence on the buffet dynamics. It has been shown through the TW approach, that for the selected wavelengths (3 and 6 cm), being close to the KH vortices wavelength (~3.5 cm) and to its first subharmonic) and actuation frequencies in the range of 250-750 Hz, inspired form previous studies in the EU-SMS project, a considerable attenuation of the Kelvin-Helmholtz (KH) vortices occurs, as well as a thinning of the separated shear layers downstream of the shock's foot. These facts have been able to allow the shock's motion to occur in farther downstream positions and to reduce the "excursion" (i.e. the shock's motion amplitude) along the suction side, with a considerable drag reduction in the order of 6 % that occurs *in nearly all cases*. This benefit has been attributed to the reduction of the shock movement fluctuation on the suction side, resulting in a high reduction in the *rms* of the aerodynamic coefficients, $\overline{C_L'}$ and $\overline{C_D'}$. The location of the TW area was starting slightly inside the area of the buffet's motion and was applied up to the trailing edge. The present study has shown a lift-to-drag increase in the order of 2.2 % mainly due to the drag reduction and not to a gain in the lift, because this location prevented the shock wave to move in a more pronounced downstream position. Therefore, the present study has shown that this concept is highly interesting to reduce the drag but it has to be applied a bit downstream of the most downstream position of the shock arising in the static (non-actuated) case.
The second morphing concept (TE region vibration and slight deformation) has shown a considerable improvement of the aerodynamic performance, especially for the angle of incidence of 1.8° and M=0.78, that is of priority interest for the design in cruise phase. This study provided a drag reduction of 14 % and a corresponding lift-to-drag increase in the order of 8 % for an actuation at 250 Hz. Once again, this has been due to the drag reduction, because simultaneously the lift was reduced. However, the present morphing has shown a lift increase in the range of (1.8, 2.5) for the angles of incidence of 1.8 and 2.4, where a significant lift increase in the order of 7.7 % has been obtained for the angle of incidence of 0° *simultaneously with a drag reduction of 3.66 %* yielding an aerodynamic efficiency in the order of 11.8 %. It has been shown that these benefits have been due to a "lock-in" mechanism that controls the buffet motion by the actuation frequency and literally mitigates the large excursion of the buffet along the suction side, emphasized in the case of 750 Hz actuation. This benefit is associated with the practical suppression of the shear layer vortices and the "sweep" of the von Kármán vortices much farther downstream. In addition, this is accompanied by a drastic reduction of the spectral energy in the order of 50 % and of suppression of the frequency peaks of the flow instabilities associated with the TE aerodynamic noise. lift-to-drag-ratio. This allows the engine to operate in less demanding regime and to reduce the needs of propulsive energy as well as the noise. Thus, the present morphing concepts are highly interesting for disruptive future aircraft design because they lead to reduction of harmful emissions in case of fuel consumption and more generally to reduction of the propulsive energy that is important regarding zero-emission systems under study concerning the H2 storage.

From the investigation of these two morphing concepts, the present study paves the way towards investigation of a hybrid morphing concept associating simultaneously the travelling waves and the trailing edge morphing, thanks to the ability of the first to provide a robust system able to reduce the drag and the second thanks to its capability to suppress the buffet and to considerably increase the lift. Therefore, the perspective opened by the present investigation is to combine these two approaches to simultaneously improve both aerodynamic coefficients by moving the zone of the travelling wave actuation beyond the shock foot and to simultaneously apply the trailing edge morphing. This association is under investigation in the European research project HORIZON-2023-PATHFINDER N° 101129952 - BEALIVE-"Bioinspired Electroactive multiscale Aeronautical Live skin" coordinated by the present research team.

Acknowledgements

The present study is a continuation beyond the European project H2020 N° 723402 SMS - "Smart Morphing and Sensing for aeronautical Configurations", https://cordis.europa.eu/project/id/723402 within the EU H2020 TEAMAERO - "Towards Effective Flow Control and Mitigation of Shock Effects in Aeronautical Applications", https://cordis.europa.eu/project/id/860909 and within the French ANR "Agence Nationale de Recherche" project EMBIA - "Electrical Multiscale Bioinspired Interfaces in Aeronautics", https://anr.fr/Project-ANR-21-CE05-0006. They thank the EU – PRACE programme for the considerable CPU hours allocation provided in our research team through the project N°2021250049, BEAMW - "Bioinspired Electroactive Aeronautics Morphing Wings," as well as the French Supercomputing Centres TGCC, CINES and CALMIP for the considerable CPU provided in this study. Specific thanks are addressed to the Computing Centre CALMIP for having made available the platform CALLISTO, https://callisto.calmip.univ-toulouse.fr/ that has been used for the Data Management Plan of this study and for the workflows elaborated through a specific Ontology for the exchange, interoperability and re-use (FAIR) of the data thanks to the contribution of T. Louge (Louge *et al.* (2023)), as well as N. Renon and J.L. Estivalezes, Director of this Centre, in the context of the DATANOOS platform (https://datanoos.univ-toulouse.fr/) coordinated by IRIT (Institut de Recherche en Informatique de Toulouse), Dr. Nathalie Aussenac and Prof. Michelle Sibilla, supported by the Foundation STAE "Sciences et Technologies pour l'Aéronautique et l'Espace, (https://www.fondation-stae.net/), where the present research team coordinates the "UseCase1", https://datanoos.univ-toulouse.fr/en/use-case-enhanced-and-intelligent-aerodynamic-modeling. Warm thanks are expressed to Drs J.L. Farges and T. Chaboud of ONERA-Toulouse for their significant contribution in the workflows permitting evaluation of the fuel's consumption obtained through the morphing. The authors are grateful to the Computing service of IMFT (Institut de Mécanique des Fluides de Toulouse), Mr. Charles Nicolas, Yannick Exposito and Emile Jamaux, for their continuous assistance for the computing facilities used in our Institute for the present study.

References

U. Antoni. « Construction of flexible aeroplane wings having a variable profile ». *US Patent* No. 1,886,362, filed August 24, 1931, issued November 8, 1932.

S. Barbarino, O. Bilgen, R. M. Ajaj, M. I. Friswell and D. J. Inman. « A review of morphing aircraft ». *Journal of Intelligent Material Systems and Structures*, 22(9):823–877, 2011. https://doi.org/10.1177/1045389X11414084.

J. D. Bartley-Cho, D. P. Wang, Christopher A. Martin, J. N. Kudva, and M. N. West. « Development of high-rate, adaptive trailing edge control surface for the smart wing phase 2 wind tunnel model ». *Journal of Intelligent Material Systems and Structures*, 15(4):279–291, April 2004. https://doi.org/10.1177/1045389x04042798.

A. Bouhadji and M. Braza. « Organised modes and shock–vortex interaction in unsteady viscous transonic flows around an aerofoil. Part I: Mach number effect ». *Journal of Computers and Fluids*, Vol. 32, Issue 9, pp. 1233–1260, 2003(a). https://doi.org/10.1016/S0045-7930(02)00100-7.

A. Bouhadji and M. Braza. « Organised modes and shock–vortex interaction in unsteady viscous transonic flows around an aerofoil. Part II: Reynolds number effect ». *Journal of Computers and Fluids*, Vol. 32, Issue 9, pp. 1261–1281, 2003(b). https://doi.org/10.1016/S0045-7930(02)00101-9 .

S. Bourdet, M. Braza, A. Bouhadji and F. Thiele. « Direct Numerical Simulation of the three- dimensional transition to turbulence in the transonic flow around a wing ». *Journal of Flow, Turbulence and Combustion*, 71:203–220, 2003. URL: https://link.springer.com/article/10.1023/B:APPL.0000014932.28421.9e .

R. Bourguet, M. Braza, G. Harran and R. El Akoury. « Anisotropic Organised Eddy Simulation for the prediction of non-equilibrium turbulent flows around bodies ». *Journal of Fluids and Structures*, 24 (8), 1240–1251, 2008. https://doi.org/10.1016/j.jfluidstructs.2008.07.004.

M. Braza, F. Auteri, P. Flaszynski, J.F. Rouchon and G. Tzabiras. « Smart Morphing and Sensing for aeronautical configurations - Prototypes, experimental and numerical findings from the H2020 N°723402 SMS EU Project ». *Notes on Numerical Fluid Mechanics and Multidisciplinary Design, Springer*, Vol. 153, 2023. https://doi.org/10.1007/978-3-031-22580-2.

M. Braza, D. Faghani and H. Persillon. « Successive stages and the role of natural vortex dislocations in three-dimensional wake transition ». *Journal of Fluid Mechanics*. 439, pp. 1-41, 2001. https://doi.org/10.1017/S002211200100458X.

M. Braza, R. Perrin and Y. Hoarau. « Turbulence properties in the cylinder wake at high Reynolds numbers ». *Journal of Fluids and Structures*, 22, pp. 757–771, 2006. https://doi.org/10.1016/j.jfluidstructs.2006.04.021.

G.L. Brown and A. Roshko. « On density effects and large structure in turbulent mixing layers ». *Journal of Fluid Mechanics*, 64(4):775–816, 1974. https://doi.org/10.1017/S002211207400190X.

V. Brunet. « Computational Study of Buflet Phenomenon with Unsteady RANS Equations ». in: 21thAIAA Applied Aerodynamics Conference. Orlando, Florida, USA, AIAA2003-3679,23–26 June 2003, https://doi.org/10.2514/6.2003-3679.

V. Brunet, S. Deck, P. Molton, M. Thiery, « A complete experimental and numerical study of the buffet phenomenon over the OAT15A airfoil », in: 40è Colloque d'Aérodynamique Appliquée, 21–23th March 2005, Toulouse, France.

G.D. Bryant and A.W. Stewart. « Variable camber airfoil ». *US Patent* No. 3,109,613, filed Nov. 28, 1960, issued Nov. 5, 1963.

L. F. Campanile and D. Sachau. « The belt-rib concept: A structronic approach to variable camber ». *Journal of Intelligent Material Systems and Structures*, 11(3):215–224, March 2000. https://doi.org/10.1106/6h4b-hbw3-vdj8-nb8a.

B. Cantwell and D. Coles. « An experimental study of entrainment and transport in the turbulent near wake of a circular cylinder ». *Journal of Fluid Mechanics*, 136:321–374, 1983.

https://doi.org/10.1017/S0022112083002189.

K.Y. Chien. « Predictions of channel and boundary-layer flows with a low-Reynolds-number turbulence model ». *AIAA journal*. 20(1), 33-38, 1982. https://doi.org/10.2514/3.51043.

M. Chinaud, A. Boussaid, J.F. Rouchon, E. Duhayon, E. Deri, D. Harribey and M. Braza. « Thermo-mechanical coupling in Nitinol. Application to an electro-morphing plate ». In *2012 XXth International Conference on Electrical Machines*, pages 2580–2584, 2012. https://doi.org/10.1109/ICElMach.2012.6350249 .

M. Chinaud, J.F. Rouchon, E. Duhayon, J. Scheller, S. Cazin, M. Marchal and M. Braza. « Trailing- edge dynamics and morphing of a deformable flat plate at high Reynolds number by time- resolved PIV ». *Journal of Fluids and Structures*, **47**, pp. 41-54, 2014. https://doi.org/10.1016/j.jfluidstructs.2014.02.007.

M. Chinaud, J. Scheller, J.F. Rouchon, E. Duhayon and M. Braza. « Hybrid electroactive wings morphing for aeronautic applications ». Solid State Phenomena, vol. 198, Trans Tech Publications, Ltd., Mar. 2013, pp. 200–205. https://doi.org/10.4028/www.scientific.net/SSP.198.200.

J. Cruz and E. J. Miller. « Evaluation of load analysis methods for NASA's GIII adaptive compliant trailing edge project ». In *54th AIAA Aerospace Sciences Meeting*. American Institute of Aeronautics and Astronautics, January 2016. https://doi.org/10.2514/6.2016-0804.

C.B. Da Silva, J.C.R. Hunt, I. Eames, J. Westerweel, 2014. « Interfacial layers between regions of different turublence intensity ». Annual Review of Fluid Mechanics 46, 567–590. https://doi.org/10.1146/annurev-fluid-010313-141357

J. Dandois, I. Mary, V. Brion, « Large-eddy simulation of laminar transonic buffet », Journal of Fluid Mechanics, 850, pp. pp. 156 - 178 2018

S. Deck. « Numerical simulation of transonic buffet over a supercritical airfoil ». *AIAA Journal*, 43 (7):1556–1566, 2005. https://doi.org/10.2514/1.9885.

I. Dimino, M. Ciminello, A. Concilio, R. Pecora, F. Amoroso, M. Magnifico, M. Scheller, A. Gratias, A. Volovick and L. Zivan. « Distributed actuation and control of a morphing wing trailing edge ». *Smart Intelligent Aircraft Structures (SARISTU)*, *Springer, Cham*, pp. 171–186, 2016. https://doi.org/10.1007/978-3-319-22413-8_9.

H. Djeridi, M. Braza, R. Perrin, G. Harran, E. Cid and S. Cazin. « Near-wake turbulence properties around a circular cylinder at high Reynolds number ». *Flow, Turbulence and Combustion.*, 71, 19–34, 2003. https://doi.org/10.1023/B:APPL.0000014930.49408.53.

P. Doerffer, P. Flaszynski, J-P- Dussauge, H. Babinsky, P. Grothe, A. Petersen, F. Billard, Sci. Eds « Transition Location Effect on Shock Wave Boundary Layer lnteraction », Notes on Numerical Fluid Mechanics and Multidisciplinary Design, 144, Publisher Springer, 2021, https://link.springer.com/book/10.1007/978-3-030-47461-4.

P. Doerffer, Ch. Hirsch, J-P. Dussauge, H. Babinsky, G. N. Barakos. « Unsteady Effects of Shock Wave induced Separation », Sci. Eds. Publisher Springer (2011) https://link.springer.com/book/10.1007/978-3-642-03004-8.

J. Donea, S. Giuliani and J.P. Halleux. « An arbitrary lagrangian-eulerian finite element method for transient dynamic fluid-structure interactions ». *Computer Methods in Applied Mechanics and Engineering*, Vol. 33, Issues 1–3, pp. 689–723, Sep. 1982. https://doi.org/10.1016/0045-7825(82)90128-1.

W. J. Duncan, L. Ellis, C. Scruton. « First report on the general investigation of tail buffeting ». Aeronaut. Research. Com. R. & M. 1457, part I, 1932.

J.L. Farges and T. Chaboud. « Aircraft trajectories, polars and fuel consumption, in Smart Morphing and Sensing for aeronautical configurations - Prototypes, experimental and numerical findings from the H2020 N°723402 SMS EU Project ». *Notes on Numerical Fluid Mechanics and Multidisciplinary Design*, *Springer*, Vol. 153, pp. 147–153, 2023. URL https://doi.org/10.1007/ 978-3-031-22580-2.

A. Favre. « Turbulence: Space-time statistical properties and behavior in supersonic flows ». *the Physics of fluids*, vol. 26, no. 10, pp. 2851-2863, 1983. https://doi.org/10.1063/1.864049.

Y.C. Fung. 2002. « An Introduction to the Theory of Aeroelasticity ». Dover, Schlieren Picture, Page 313 by D. W. Holder, National Physical Laboratory, UK.

T.B. Gatski and C.G. Speziale. « On explicit algebraic stress models for complex turbulent flows ». *Journal of fluid and Mechanics*. 1993; 254:59-78. https://doi.org/10.1017/S0022112093002034.

F. Grossi, M. Braza and Y. Hoarau. « Prediction of transonic buffet by Delayed Detached-Eddy Simulation ». *AIAA Journal*, 52, N°10, 2014, pp. 2300-2312. https://doi.org/10.2514/1.J052873.

W. Haase, M. Braza and A. Revell. « DESider - A European effort on hybrid RANS-LES modelling ». *Notes on Numerical Fluid Mechanics and Multidisciplinary Design*, 103:2300–2312, 2009. https://doi.org/10.1007/978-3-540-92773-0.

Y. Hoarau. « *Analyse physique par simulation numérique et modélisation des écoulements décollés instationnaires autour de surfaces portantes* ». PhD thesis, INPT 2002. URL https://www.theses.fr/2002INPT013H.

Y. Hoarau, D. Pena, J.B. Vos, D. Charbonier, A. Gehri, M. Braza, T. Deloze and E. Laurendeau. « *Recent Developments of the Navier Stokes Multi Block (NSMB) CFD solver* ». *Book title: 54th AIAA Aerospace Sciences Meeting*. 2016. https://doi.org/10.2514/6.2016-2056.

J. C. R. Hunt, I. Eames and J. Westerweel. « Vortical interactions with interfacial shear layers ». pages 331–338, 2008. http://dx.doi.org/10.1007/978-1-4020-6472-2_50

A. K. M. F. Hussain and W. C. Reynolds. « The mechanics of an organized wave in turbulent shear flow ». *Journal of Fluid Mechanics*, 41(2):241–258, 1970. https://doi.org/10.1017/S0022112070000605.

L. Jacquin, P. Molton, S. Deck, B. Maury and D. Soulevant. « Experimental study of shock os- cillation over a transonic supercritical profile ». *AIAA Journal*, 47(9):1985–1994, 2009. https://doi.org/10.2514/1.30190.

L. Jacquin, P. Molton, S. Deck, B. Maury and D. Soulevant. « An experimental study of shock oscillation over a transonic supercritical profile ». *In 35th AIAA Fluid Dynamics Conference and Exhibit, Toronto, Ontario, Canada, AIAA* 2005-4902, 6–9 June.

A. Jameson. « Energy Estimates for Nonlinear Conservation Laws with Applications to Solutions of the Burgers Equation and One-Dimensional Vicous Flow in a Shock Tube by Central Difference Schemes ». 18th AIAA 2007 Computational Fluid Dynamics Conference, Miami. https://doi.org/10.2514/6.2007-4620

A. Jimenez-Garcia, « Etude de l'interaction tremblement transsonique – instabilité de von Kármán à l'aide d'une plaque de bord de fuite par approche de modélisation de la turbulence statistique avancée », Master thesis, ENSEEIHT Engineering School and Institut de Mécanique des Fluides de Toulouse, (IMFT) http://smartwing.org/SMS/EU/DOCUMENTS/Antonio_JIMENEZ_GARCIA.pdf, 2012.

C. Jimenez-Navarro, J.B. Tô, C. Rouaix, P. Flaszynski, P. Kaczynski, P. Doerffer, A. Marouf, R. El Akoury, Y. Hoarau, J.F. Rouchon and M. Braza. « Morphing effects on the aerodynamic performances of a supercritical wing's prototype in transonic flow conditions ». *Advanced Computational Methods and Design for Greener Aviation, Computational Methods in Applied Sciences, ECCOMAS-Springer in print*, 2022.

G. Jin and M. Braza. « Two-equation turbulence model for unsteady separated flows around airfoils ». *AIAA Journal*, 32, N° 11, Nov. 1994, pp. 2316-2320. https://doi.org/10.2514/3.12292.

G. Jodin. « Hybrid electroactive morphing at real scale - application to airbus A320 wings », 2017. URL https://www.theses.fr/2017INPT0093. PhD thesis, Toulouse, INPT 2017.

S. Kota, P. Flick and F. S. Collier. « *Flight Testing of FlexFloil^{TM} Adaptive Compliant Trailing Edge* ». *54th AIAA Aerospace Sciences Meeting*. American Institute of Aeronautics and Astronautics, January 2016. https://doi.org/10.2514/6.2016-0036.

R. LeLetty, N. Lehermet, G. Patient, F. Claeyssen and M. Lang. « Valves Based on Amplified Piezoelectric Actuators ». NanoTech 2002 - "At the Edge of Revolution". https://doi.org/10.2514/6.2002-5715.

L.L. Levy. « Experimental and computational steady and unsteady transonic flows about a thick airfoil ». *AIAA Journal*, 16(6):564–572, 1978. https://doi.org/10.2514/3.60935.

T. Louge, J.B. Tô, C. Jimenez-Navarro, A. Marouf and M. Braza. « Data sharing of SMS and Workflows through Ontology-Based Data Access in the Platform CALMIP/CALLISTO, in Smart Morphing and Sensing for aeronautical configurations - Prototypes, experimental and numerical findings from the H2020 N°723402 SMS EU Project ». *Notes on Numerical Fluid Mechanics and Multidisciplinary Design, Springer*, Vol. 153, pp. 256–267, 2023. URL https://doi.org/10.1007/ 978-3-031-22580-2.

Z. Lyu and J. R. R. A. Martins. « Aerodynamic shape optimization of an adaptive morphing trailing- edge wing». *Journal of Aircraft*, 52(6):1951–1970, 2015. https://doi.org/10.2514/1.C033116.

A. Marouf, N. Simiriotis, J. B. Tô, Y. Bmegaptche, Y. Hoarau, and M. Braza. « DDES and OES Simulations of a Morphing Airbus A320 Wing and Flap in Different Scales at High Reynolds number ». In Y. Hoarau, Shia-Hui Peng, D. Schwamborn, A. Revell, and C. Mockett, Sci. Eds. Progress in Hybrid RANS-LES Modelling. 2020, pp. 249–258, Publisher Springer, https://doi.org/10.1007/978-3-030-27607-2_20

J. G. Marvin, L. L. Levy and H. L. Seegmiller. « Turbulence modeling for unsteady transonic flows ». *AIAA Journal*, 18(5):489–496, 1980. https://doi.org/10.2514/3.50782.

J.B. McDevitt, L.L. Levy and G.S. Deiwert. « Transonic flow about a Thick Circular-Arc Airfoil ». *AIAA Journal*, 14(5):606–613, 1976. https://doi.org/10.2514/3.61402.

A.-M.R. McGowan, W.K. Wilkie, R.W. Moses, R.C. Lake, J.L. Pinkerton-Florance, C.D. Weiseman, M.C. Reaves, B.K. Taleghani, P.H. Mirick and M.L. Wilbur. « Aeroservoelastic and structural dynamics research on smart structures conducted at NASA Langley Research Center ». In Smart Structures and Materials 1998: Industrial and Commercial Applications of Smart Structures Technologies, vol. 3326, pp. 188-201. SPIE, 1998. https://doi.org/10.1117/12.310634.

DG MOVE/ DG RTD, « Flightpath 2050: Europe's Vision for Aviation: Maintaining global leadership and serving society's needs », European Commission Publications Office 2012, https://data.europa.eu/doi/10.2777/15458

H. Namgoong, W.A. Crossley and A.S. Lyrintzis. « Aerodynamic optimization of a morphing airfoil using energy as an objective ». *AIAA Journal*, 45(9):2113–2124, 2007. https://doi.org/10.2514/1.24355.

E. Paladini, S. Beneddine, J. Dandois, D. Sipp, J.C. Robinet. « Transonic buffet instability: From two-dimensional airfoils to three-dimensional swept wings ». Physical Review Fluids, 2019, 4 (10), pp.103906. https://link.aps.org/doi/10.1103/PhysRevFluids.4.103906, hal-02455164

H.F. Parker. « Variable camber rib for aeroplane wings ». *US Patent* 1,341,758, filed July 17, 1919, issued June 1, 1920.

R. Pecora, F. Amoroso and M. Magnifico. « Toward the bi-modal camber morphing of large aircraft wing flaps: the CleanSky experience ». Vol. 9801, pp. 98–106, 2016. https://doi.org/10.1117/12.2218415.

R. Perrin, M. Braza, E. Cid, S. Cazin, A. Barthet, A. Sevrain, C. Mockett and F. Thiele. « Obtaining phase averaged turbulence properties in the near wake of a circular cylinder at high Reynolds number using POD ». *Experiments in Fluids*, 43, pp. 341–355, 2007. https://doi.org/10.1007/s00348-007-0347-6.

R. Perrin, M. Braza, E. Cid, S. Cazin, P. Chassaing, C. Mockett, T. Reimann and F. Thiele. « Coherent and turbulent process analysis in the flow past a circular cylinder at high Reynolds number ». *Journal of Fluids and Structures*, 24(8), 1313–1325, 2008. https://doi.org/10.1016/j.jfluidstructs.2008.08.005.

PL. Roe. « Approximate Riemann solvers, parameters vectors and difference schemes ». *Journal of Computational Physics*, 43, 1981. ISSN 0021-9991. https://doi.org/10.1016/0021-9991(81)90128-5 .

T. Rung, U. Bunge, M. Schatz, F. Thiele, « Restatement of the Spalart-Allmaras Eddy-Viscosity Model in Strain-

Adaptive Formulation » *AIAA Journal*, 41, No7, 2003, pp.1396–1399.

J. Scheller. « Electroactive morphing for the aerodynamic performance improvement of next generation airvehicles ». Ph.D. thesis, Toulouse: INPT-IMFT. October 2015. https://oatao.univ-toulouse.fr/14479/.

J. Scheller, M. Chinaud, J.F. Rouchon, E. Duhayon, S. Cazin, M. Marchal and M. Braza. « Trailing- edge dynamics of a morphing NACA0012 aileron at high Reynolds number by high-speed PIV ». *Journal of Fluids and Structures*, 55, pp. 42–51, 2015. https://doi.org/10.1016/j.jfluidstructs.2014.12.012 .

J. Scheller, G. Jodin, K.J Rizzo, E. Duhayon, J.F. Rouchon, M. Triantafyllou and M. Braza. « A combined smart-materials approach for next-generation airfoils ». *Solid-State Phenomena*, **251**, pp. 106-112, 2016. 10.4028/www.scientific.net/SSP.251.106.

H.L. Seegmiller, J.G. Marvin and L.L. Levy. « Steady and Unsteady Transonic Flow ». *AIAA Journal*, 16(12):1262–1270, 1978. https://doi.org/10.2514/3.61042.

N. Simiriotis, G. Jodin, A. Marouf, P. Elyakime, Y. Hoarau, J.C. Hunt, J.F. Rouchon and M. Braza. « Morphing of a supercritical wing by means of trailing edge deformation and vi- bration at high Reynolds numbers: Experimental and numerical investigation ». *Journal of Fluids and Structures*, 91, 2019. https://doi.org/10.1016/j.jfluidstructs.2019.06.016 .

D. Szubert, I. Asproulias, N. Simiriotis, J.B. Tô, V. Temtching-Temou, Y. Hoarau and M. Braza. « Numerical simulation of 3-D laminar wing ». *In Book: Transition Location Effect on Shock Wave Boundary Layer lnteraction, Series: Notes on Numerical Fluid Mechanics and Multidisciplinary Design, Sci. Eds*. P. Doerffer, P. Flasynski, J-P- Dussauge, H. Babinsky, P. Grothe, A. Petersen, F. Billard, Publisher Springer, **144**, Publisher Springer**,** 2021.

D. Szubert, F. Grossi, A. Jimenez-Garcia, V. Guibert, Y. Hoarau, S. Saintlos, J. Hunt and M. Braza. « Feedback effects and stochastic forcing response of the transonic buffet around an airfoil including trailing-edge-plate at high Reynolds ». ECCOMAS Conference, Vienna, September 2012.

D. Szubert, F. Grossi, A. Jimenez-Garcia, Y. Hoarau, J.C.R. Hunt and M. Braza. « Shock-vortex shear-layer interaction in the transonic flow around a supercritical airfoil at high Reynolds number in buffet conditions ». *Journal of Fluids and Structures*, 55, pp. 276–302, 2015. https://doi.org/10.1016/j.jfluidstructs.2015.03.005.

S. A. Tawfik, D. S. Dancila, and E. Armanios. « Unsymmetric composite laminates morphing via piezoelectric Actuators ». *Composites Part A: Applied Science and Manufacturing*, 42(7):748–756, July 2011. https://doi.org/10.1016/j.compositesa.2011.03.001.

J. B. Tô, N. Simiriotis, A. Marouf, D. Szubert, I. Asproulias, D.M. Zilli, Y. Hoarau, J.C.R. Hunt and M. Braza. « Effects of vibrating and deformed trailing edge of a morphing supercritical airfoil in transonic regime by numerical simulation at high Reynolds number ». *Journal of Fluids and Structures*, 91, 2019. https://doi.org/10.1016/j.jfluidstructs.2019.02.011.

B. van Leer. « Towards the ultimate conservative difference scheme. V.A second-order sequel to Godunov's method ». *Journal of Computational Physics*, 32(1):101–136, 1979. ISSN 0021-9991. https://doi.org/10.1016/0021-9991(79)90145-1 .

S. Venkateswaran and C. Merkle. « Dual time-stepping and preconditioning for unsteady computations ». Book title: 33rd aerospace sciences meeting and exhibit. American institute of aeronautics and astronautics. 1995. https://doi.org/10.2514/6.1995-78 .

J. Vos, A. Rizzi, A. Corjon, E. Chaput and E. Soinne. « Recent advances in aerodynamics inside the nsmb (navier stokes multi block) consortium ». *36th AIAA Aerospace Sciences Meeting and Exhibit*, 1998. https://doi.org/10.2514/6.1998-225.

B. KS. Woods and M. I Friswell. « Multi-objective geometry optimization of the fish bone active camber morphing airfoil ». *Journal of Intelligent Material Systems and Structures*, 27(6):808–819, September 2015. https://doi.org/10.1177/1045389x15604231.

P. C. Wölcken and M. Papadopoulos, editors. « Smart Intelligent Aircraft Structures (SARISTU) ». *Springer International Publishing*, 2016. https://doi.org/10.1007/978-3-319-22413-8.

E.J. Zapel. « Variable camber trailing edge for airfoil ». *US Patent* No. 4,131,253, filed July 21, issued Dec. 26, 1978.

A. Zhao, H. Zou, H. Jin and D. Wen. « Structural design and verification of an innovative whole adaptive variable camber wing ». *Aerospace Science and Technology*, 89:11-18, June 2019. https://doi.org/10.1016/j.ast.2019.02.032.